Multiset Neurons

Luciano da Fontoura Costa

Multiset Neurons

Luciano da Fontoura Costa
luciano@ifsc.usp.br

São Carlos Institute of Physics – DFCM/USP

1st Nov. 2021

Abstract

The present work reports a comparative performance of artificial neurons obtained in terms of the real-valued Jaccard and coincidence similarity indices and respectively derived functionals. The interiority index and classic cross-correlation are also included for comparison purposes. After presenting the basic concepts related to real-valued multisets and the adopted similarity metrics, including the generalization of the real-valued Jaccard and coincidence indices to higher orders, we proceed to studying the response of a single neuron, not taking into account the output non-linearity (e.g. sigmoid), respectively to the detection of gaussian two-dimensional stimulus in presence of displacement, magnification, intensity variation, noise and interference from additional patterns. It is shown that the real-valued Jaccard and coincidence approaches are substantially more robust and effective than the interiority index and the classic cross-correlation. The coincidence-based neurons are shown to have the best overall performance respectively to the considered type of data and perturbations. The potential of the multiset neurons is further illustrated with respect to the challenging problem of image segmentation, leading to impressive cost/benefit performance. The reported concepts, methods, and results, have substantial implications not only for pattern recognition and machine learning, but also regarding neurobiology and neuroscience.

1 Introduction

A great deal of human perception and cognition, as well as of many other living beings, critically rely on neuronal transduction and processing of several types of information. From a simplified mathematical perspective, a neuron has been understood as a cell specialized in processing and transmitting signals. In a very simplified approach to modeling neuronal operation, known as *integrate-and-fire*, neuronal dynamics can be though as involving the two following main stages: (i) *integration:* an inner product between the input stimulus and the respective synaptic weights, yielding an accumulated value; and (ii) *fire:* the subsequent application of a non-linear function, such as a sigmoid, over that value, eventually yielding an action potential (e.g. [1, 2]).

This type of operation can be complemented, regarding the geometrical/shape aspects of neuronal operation, in terms of the concept of *receptive field* (e.g. [3, 4]) defined with respect to some input stage space. For instance, several of the ganglion cells of the retina (e.g. [5]) have been characterized by respective antagonic receptive fields defined on the visual space (scene) or along the retina surface (retinotopic). Cortical neuronal cells often operate on topographical mappings of the visual field (e.g. [3, 4]). The mathematical modeling of these receptive fields therefore provides an effective manner for representing, modeling, and better understanding neuronal operation according to a systemic representation which is directly related to the concepts of correlation, convolution and point-spread functions (e.g. [6, 7, 8, 9]).

In addition to its dynamic properties along time, the shape of receptive fields has been understood to play an important role in detecting and processing patterns. Indeed, a more elaborated dendritic arborization will tend to have enhanced chances of receiving more synaptic connections. The importance of the neuronal geometry seems to be so important that it often adapts to the type of function the neuron performs (e.g. [10, 11, 12]). Among the several possible interrelationships between neuronal shape and function, we have that the alignment and similarity between the visual signal and the neuronal two-dimensional distribution of synaptic weights tend to result in higher neuronal activation, therefore providing some kind of *template matching* or *matched filtering*.

In the present work, we re-evaluate the functioning of single neurons in terms of recently introducted multiset-based similarity indices capable of operating on real-valued data [13, 14]. More specifically, instead of using the traditional inner product, we apply the real-

valued Jaccard, interiority, and coincidence similarity metrics [13, 14, 15].

Introduced decades ago [16], the Jaccard similarity between two sets A and B is aptly defined in terms of the following ration between set operations:

$$\mathcal{J}(A,B) = \frac{|A \cap B|}{|A \cup B|} \tag{1}$$

where $|A|$ stands for the cardinality of set A, and $0 \leq \mathcal{J}(A,B) \leq 1$.

When extended to 1D densities or non-negative functions (e.g. [17, 18, 14, 13]), the Jaccard index can be understood in particularly appealing geometrical manner as the ratio between the area shared between the two functions and the union of their respective areas. Of particular interest is the fact that, though extremely simple, the Jaccard index implements an action that, though analogous to the classic inner product, is non-linear as a consequence of the use of the maximum and minimum binary operators which are, in multiset theory (e.g. [19, 20, 21, 22, 23, 24]), required for union and intersection of multisets, respectively. By 'binary operator' it is meant the mathematical understanding of an operation involving two arguments.

Though the present work focuses on the use of multiset similarities respectively to biological and artificial neurons, the several analysis and comparisons with other operators provide interesting resoures regarding other applications of the real-valued Jaccard and coincidence operators, be it used as quantifications of similarity (e.g. [13]) or as the means to translated datasets into respective networks (e.g. [15]).

We start by presenting the inner product, its properties, basic multiset concepts (e.g. [19, 20, 21, 22, 23, 24]), as well as the recently introduced real-valued Jaccard and coincidence indices [13, 18, 14]. This presentation is performed first respectively to one-dimensional input, and then extended to two- and multidimensional synaptic inputs. In addition to discussing the intrinsic, though limited, ability of the real product between two scalars in providing information about their respective similarity, we also show how the real-valued Jaccard index can be derived in a logical manner starting from the totally strict similarity comparison provided by the Kronecker delta function.

Unlike in a recent study [13], which approached the subject of similarity more generally in terms of correlation-like perspective, the neuronal perspective adopted in this work allowed attention to be focused on similarity comparisons where one of the arguments is kept constant, therefore corresponding to stable synaptic weights. In addition, for generality's sake, additional results are reported regarding the generalization of the multiset similarity indices to higher orders, yielding a generic similarity function that converges to the Kronecker delta product for infinite order.

A systematic approach is then proposed and applied for comparing the performance of neurons in pattern recognition, while adopting the standard cross-correlation as well as the interiority, real-valued Jaccard and coincidence indices [13, 18, 14]. The comparison is performed with respect to varying pattern position, intensity, scale, noise levels, presence of additional interfering patterns, and false positives resulting from completely noisy data.

Several interesting results are report that, all in all, confirm that the coincidence index provides the most strict and detailed recognition, followed by the real-valued Jaccard and interiority indices. The classic cross-correlation resulted almost useless for the considered task and type of data. These results have many implications and applications to several related areas, some of which are also briefly discussed.

2 The Importance of Feature Spaces

The type of input received by a neuronal cell (biological or artificial) — including the respective physical units, mutual interrelationship, and coordinate system (basis chosen for representation) — has a critically important impact on subsequent processing, including pattern recognition. Henceforth we will understand each individual synaptic input to a neuronal cell as being associated to a respective *measurement* or *feature*, which can often be modeled as a random variable.

Figure 3 depicts two main situations regarding the type of input received by a neuronal cell (biological or artificial). In Figure 3(a), we have a single neuronal cell deriving its synaptic input directly from the coordinates of geometric data organized topographically, in which case there are intrinsic geometrical relationships (e.g. continuity and proximity) implied by proximity and adjacency between the data elements or features that constitute potentially useful information for the neuronal processing. An example of this type of input is the description of the geometry of a 3D real-world object (e.g. an apple) in terms of the respective position of each of its points, each of them corresponding to as defined by an orthonormal coordinate system. Observe that each of these features have completely homogeneous, having exactly the same nature (physical unit of space). In these cases, geometric transformations such as translations, rotation, and eventually scaling (e.g. citeshapebook) are well posed, and the recognition is often required to be performed invariant to these transformations.

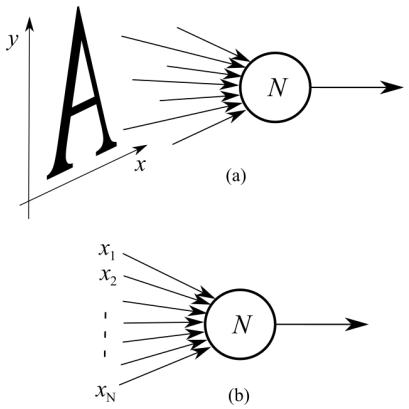

Figure 1: The two main types of synaptic inputs to an individual neuronal cell: (a) the features have homogeneous units, corresponding to the positions (coordinates) of the points of the patterns to be recognized, in the case of this particular example being measured in 2D orthogonal coordinate system (the x and y coordinates of each of the pattern points are taken as respective synaptic input/feature); (b) the features are of more general and heterogeneous and potentially abstract and/or compound nature, such as temperature, color, weight, age, value, etc. Observe that any feature may correspond to a functional combination and/or composition of the others, while other features are more independent one another. In practice, the identification of the intrinsic mathematical structure of the adopted features constitutes a rather challenging issue.

However, the above discussed geometrical type of input is never verified in biological or machine recognition systems, except for situations in which the neurons operate directly onto the visual scene projections onto the retina, but in this case the coordinate system is no longer orthogonal or normalized (projection from 3D to 2D). In visual pattern recognition systems, except for the first layer receiving projections of the scene, the neuronal input almost invariably relate to measurements – such as sizes, angles, areas, etc. — that are derived from the patterns geometry but not correspond directly to the individual position of the object points in an orthogonal system.

Figure 3(b) shows another situation, much more frequently observed in practice regarding neuronal input. Here, though the position of each feature is important, they have heterogenous units and are not directly related coordinate systems are rather unlikely to be orthonormal, so that invariance to rigid body transformations are unlikely to be meaningful (or viable) for neuronal response. For instance, the synaptic input of a specific neuronal cell may involve, respectively to the pattern being analyzed, its color, temperature, weight, speed, etc. These features are rather unlikely to belong to a orthonormal coordinate system. A better appreciation of this important effect can be obtained by considering that each feature corresponds to a measurement that may potentially be related to the other adopted features. These relationships can be linear, such as when one of the features corresponds to a linear combination of other features taken or not into account, or even non-linear combinations and compositions of features.

Figure 2 illustrates the prototypical orthonormal system in 3D, which provide an ideal reference for synaptic input, though this is almost never observed in practical situations. An example of real-world situation involving this type of feature representations corresponds to the positions of objects in the 3D space, measured by some accurate position acquisition device. Observe that this cannot be accomplished biologically, in the case of visual input, often rely on projections of 3D onto 2D, being feasible only by using artificial systems.

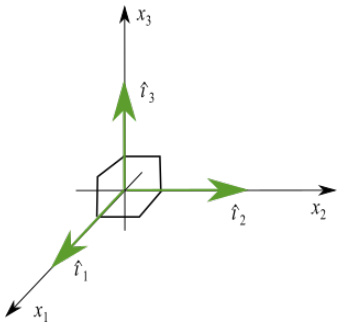

Figure 2: The $\mathcal{R}^3$ vector space, characterized by three coordinates x_1, x_2 and x_3 associated to respective *versors* $\hat{\boldsymbol{\imath}}_1$, $\hat{\boldsymbol{\imath}}_2$, $\hat{\boldsymbol{\imath}}_3$. The two vectors (blue and red) are assumed to be entirely contained in the plan $(0, x_2, x_3)$. Each generic vector $\vec{v}$ in this space can be represented as $[x_1, x_2, x_3]^T = x_1\hat{\boldsymbol{\imath}}_1 + x_2\hat{\boldsymbol{\imath}}_2 + x_3\hat{\boldsymbol{\imath}}_3$.

An important feature of the $\mathcal{R}^3$ space is the *orthonormality of the axes*, corresponding to $\langle\hat{\boldsymbol{\imath}}_1, \hat{\boldsymbol{\imath}}_2\rangle = \langle\hat{\boldsymbol{\imath}}_2, \hat{\boldsymbol{\imath}}_3\rangle = \langle\hat{\boldsymbol{\imath}}_1, \hat{\boldsymbol{\imath}}_3\rangle = 0$ (orthogonal) and $\langle\hat{\boldsymbol{\imath}}_1, \hat{\boldsymbol{\imath}}_1\rangle = \langle\hat{\boldsymbol{\imath}}_2, \hat{\boldsymbol{\imath}}_2\rangle = \langle\hat{\boldsymbol{\imath}}_3, \hat{\boldsymbol{\imath}}_3\rangle = 1$ (normalization). An example of orthonormal basis for $\mathcal{R}^3$, known as *canonical*, is as follows:

$$\hat{\boldsymbol{\imath}}_1 = [1, 0, 0]\,; \quad \hat{\boldsymbol{\imath}}_2 = [0, 1, 0]\,; \quad \hat{\boldsymbol{\imath}}_3 = [0, 0, 1] \qquad (2)$$

In practice, patterns are characterized by a set of respective features x_i, $i = 1, 2, \ldots, N$ that are pre-specified or chosen in a relatively intuitive manner, sometimes with some assistance of statistical methods such as principal component analysis (PCA, e.g. [25]). Each of these features are typically understood as defining each of the axis in the associated $N-$dimensional *feature space*, allowing each pattern to be mapped into a respective vector in this space.

A critical problem not often realized, taken into account or studied, regards the fact that the so obtained feature spaces *are almost invariably non-orthonormal* as a consequence of several effects.

Figure 3 illustrates one such situation in which the patterns to be analyzed are originally in an orthonormal

space $[x_1, x_2, x_3]$, where distances and geometric transformations such as rotation are well defined and stable. Observe that these original features do not need to correspond to space, or even have the same physical units. Two possible patterns are illustrated in terms of the blue and red vectors which, for simplicity's sake, are assumed to belong to the plan $[x_1 = 0, x_2, x_3]$. The dashed circle illustrates the position of the blue vectors that are at distance d from the red vector. As a consequence of the orthonormality of the system $[x_1, x_2, x_3]$, these positions define a perfect circle, reflecting the isometry and rotational invariance of distance in an orthogonal coordinate system. In the context of neuronal networks and pattern recognition, this circular area can be immediately be related to the concept of generalization of the reference pattern corresponding to the red vector.

However, in practice the measurements are adopted in a mostly intuitive manner while taking into account the potential of each of them for characterizing and discriminating between the available patterns. As such, it is highly unlikely that the adopted features will correspond to an orthonormal coordinate system. In the specific case in Figure 3, one of the adopted features actually corresponds to a linear combination of two of the original coordinates, e.g. $\tilde{x}_3 = 2x_3 + x_2$. Other situations undermining the orthonormality of the feature space include scaling of the original features or non-linear transformations of their individual or combined values.

In practice, the adopted features are often understood, for simplicity's sake, to be associated to an orthonormal feature space, as illustrated in Figure 3(d,e). This approach, which is characteristic to a large range of approaches in pattern recognition and neuronal networks, will be henceforth referred to as the *Cartesian surmise*.

Though the measurement values will remain property represented in each corresponding axis, it is no longer valid to assume rotational invariance or distance preservation respectively to the original, real measurements $[x_1, x_2, x_3]$. In Figure 3, this is illustrated by the fact that the isometric distance circle having become a deformed region that, in this specific case, corresponds to a shape more complex than an ellipsis, which would be otherwise obtained in case the original features had only been scaled. Even though generalization is still catered for, it is no longer isometric and by no means correspond to a circle or sphere.

One of the most immediate consequences of the critically important effects of the Cartesian surmise concerns the fact that, unless the adopted measurements do related directly to an orthonormal coordinate system, it makes little sense to expect or implement rotational invariance in the neuronal operation because, even if this property is observed in the adopted feature space, therefore defining isometric relationships between the vectors associated to the patterns, this by no means translate to the original properties of the system. Ideally, in the rather unlikely case the interrelationship between the adopted and originally orthonormal features is known, the neurons can have their operation designed so as to compensate for the respective divergences from orthonormality. At the same time, it does not by any means follows that the neuronal operation can have any erratic generalization regarding the respectively implemented quantification of similarity, in the sense that relatively symmetric generalization regions should be sought, though not necessarily corresponding to perfect spheres. Actually, other potentially more important requirements can be taken into account while defining the neuronal basic operation, such as minimizing the sensitivity of the neuronal output respective to perturbations of a single or small set of features, or normalizing with respect to the input signal overall magnitude.

3 Product and Similarity

Given any two real values x and y, their product constitutes one of the most frequently performed algebraic operation in science and technology, not to mention daily activities. Yet, there are some quite interesting properties of the product xy that, perhaps as a consequence of being so ubiquitous, are not commonly realized.

Let's start with the product sign rule:

$sign\{x\}$	$sign\{y\}$	$sign\{xy\}$
$-$	$-$	$+$
$-$	$+$	$-$
$+$	$-$	$-$
$+$	$+$	$+$

Logically, the above rules can be conceptualized as the *identity* operation of Boolean Algebra (e.g. [19]).

It follows that the classic product between two real values is capable of expressing whether the two values x and y head toward the same direction along the real line, in which case $sign\{xy\} = +1$, or if they oppose one another, yielding $sign\{xy\} = -1$. As such, the product operation can be understood to quantify, in its signal, the similarity of the relative orientations of the two operands.

This important property of the classic real product hints at a yet more important respective feature, namely the fact that *the classic real product provides measurement of similarity* between the *signs* (or direction) of two signed values x and y [13]. This particular feature of the product contributes strongly to capacity of the inner product for quantifying the similarity between two

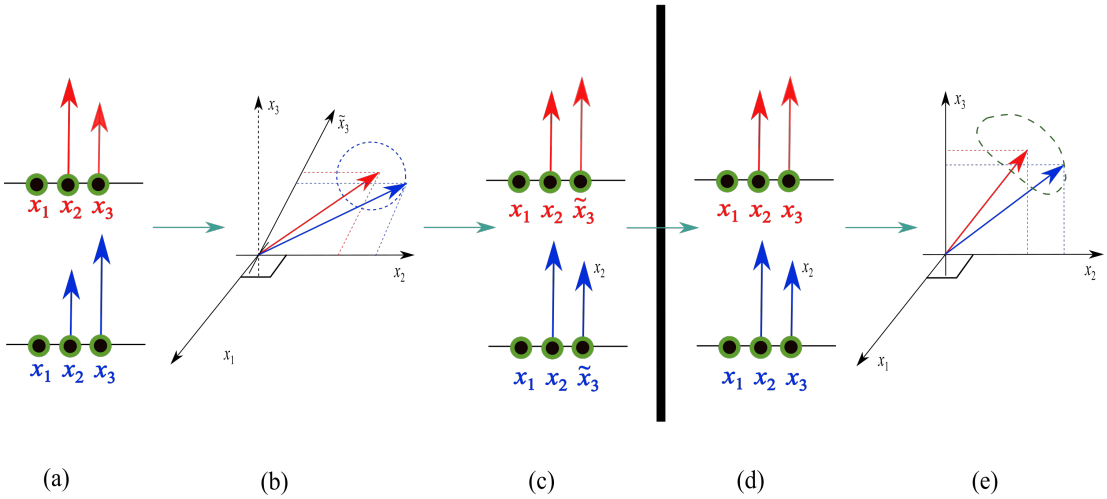

Figure 3: The *Cartesian surmise*: A real-world or abstract system (a) in which three original properties x_1, x_2 and x_3 associated to an orthogonal coordinate system (b) characterize the patterns to be studied. However, the measurements are performed respectively to a different, sheared coordinate system involving x_1, x_2 and $\tilde{x}_3$ (c) and then treated as if belonging to an orthogonal coordinate system (d,e). The horizontal bar represents the separation between the pattern and analysis domains. Though each of the individual measurement values will be preserved, respective interrelationships such as distances and magnitudes, including rotational invariance and generalization regions, can become strongly modified or invalidated.

vectors. More specifically, the traditional inner product between any two vectors $\vec{v}$ and $\vec{p}$ in an $N-$dimensional space can be written as:

$$\langle \vec{v}, \vec{p} \rangle = \sum_{i=1}^{N} v_i p_i = |\vec{v}|\,|\vec{p}| \cos(\theta) \tag{3}$$

where θ is the smallest angle between the two vectors. Provided the magnitudes of $\vec{v}$ and $\vec{p}$ are kept constant, the inner product will provide an indication of the angular and orientation similarity between these two vectors. Observe that the inner product is a bilinear operation.

When translated to scalar values, the inner product becomes:

$$\langle x, y \rangle = xy = |x|\,|y| \cos(\theta) \tag{4}$$

which makes it clear that the scalar version of the inner product is the product of the two scalar arguments.

In this case, the cosine similarity becomes:

$$\cos(\theta) = \frac{\langle x, y \rangle}{|x||y|} = \frac{xy}{|x||y|} = \pm 1 \tag{5}$$

Observe also that, provided $|x| \leq 1$ and $|y| \leq 1$, it will follow that $-1 \leq xy \leq 1$.

In the case of $\vec{x}$ and $\vec{y}$ being vectors in $\mathcal{R}^N$, the respective cosine similarity can be expressed as:

$$\cos(\theta) = \frac{\langle \vec{x}, \vec{y} \rangle}{|\vec{x}|\,|\vec{y}|} \tag{6}$$

This expression implies that the cosine similarity between two vectors can be understood as corresponding to a normalized version of the inner product between those two vectors. As a consequence, the inner product between two *versors* (vectors with unit magnitude) is identical to the respective cosine similarity.

Despite its intrinsic ability for quantifying similarity between the sign of values, as well as it extensive application in operations as the inner product, the real product has two important shortcomings. First, it is relatively difficult to be implemented in computational hardware or even in analog circuits. Second, it has been shown that the real product tends to be too tolerant regarding the provided indication of similarity [14, 13, 26], as illustrated in Figure 4 with respect to comparison between versors.

The substantially high similarity values generated by the inner product similarity between two vectors immediately implies that that it tends to provide a relatively coarse, or little strict, quantification of the relationship between the two vectors. Another feature of particular interest in the similarity profiles such as those in Figure 4 concerns the quality factor (in analogy with filter theory, e.g. [27]) of the quantification, which can be understood as being proportional to the peak value divided by the standard deviation or other dispersion measurements, therefore providing an indication of the sharpness of the profile. Another important property of a similarity profile is its magnitude of the derivative at and around its peak. Regarding the former, we have that it is zero for the inner product similarity (as expected with any smooth function) and infinite for the coincidence. At the same time, the magnitude of the derivatives around the

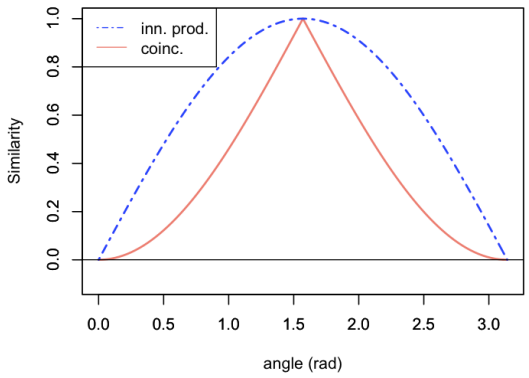

Figure 4: The pairwise similarity between versors in $\mathcal{R}^2$ as quantified by the inner product (dashed blue) and coincidence (solid salmon) similarities. The versor $\vec{x} = [0, 1]$ is compared to versors making angles from 0 to π with the horizontal axis. As expected, both similarity indices reach their respective peak at $\pi/2$, but the inner product similarity, which in the case of versors is identical to the cosine similarity, is markedly less strict in comparing similarity, providing substantially higher values than the coincidence similarity in all cases except for angles 0 and $\pi/2$.

peak are very small in the case of the inner product similarity, and particularly high for the coincidence similarity. The fact that the derivative of the coincidence similarity profile diverge at its peak can be easily circumvented, if necessary for analytical and theoretical studies, by representing the profile in terms of a truncated Fourier series, which is necessarily analytical (has any derivative).

One problem of having a smooth (or 'blunt') similarity peak, as is the case with the inner product similarity, consists in the fact that the identification of its position by using derivative is highly susceptible to any level of noise. That is so because the derivatives at and around the peak have very small magnitudes (smooth) and can therefore be severely disturbed by the noise during the derivative, as this operation emphasized the high frequency content of the curve. The sharp and intense derivative peak resulting from the coincidence can hardly have its correct position disturbed by any reasonable level of signal noise.

On the other hand, a smoother similarity comparison profile tends to favor *generalization* of the comparison, a property that is often expected at some level in neuronal networks and pattern recognition. In the case of Figure 4, the relatively higher similarity values provided by the inner product, respectively to the coincidence, similarity means that input patterns that are more different to the one used as a reference (or template) will imply larger similarity values, therefore implying larger generalization. Observe that the generalization property is opposite to accuracy in the similarity comparison, which means that either one of these two properties is prioritized, or a suitable balance between them needs to be achieved. To any extent, as it can be appreciated from Figure 4, the coincidence similarity already presents a substantial ability for generalization, yielding substantially high (though much smaller than the cosine similarity) for input with angles reasonably near $\pi/2$.

Table 1 provides a qualitative relative comparison between the several properties respectively characterizing the inner product (or cosine) and coincidence similarities.

property	inner product	coincidence
values	typ. higher	typ. lower
peak shape	smooth	sharp
peak concavity	convex	concave
strictness	lower	higher
peak localiz. accur.	lower	higher
magn. deriv. at peak	lower	higher
deriv. at peak	0	∞
quality factor	lower	higher
false neg. prob.	lower	higher
false pos. prob.	higher	lower
generalization	higher	lower
complexity	higher	lower

Table 1: Relative comparison of the main properties of the inner product (cosine) and coincidence similarities. The abbreviation *peak localiz. accur.* means peak localization accuracy, and the term *complexity* property related to conceptual and implementation (software or hardware) aspects.

However, being more or less strict does not necessarily imply an advantage or shortcoming of a given similarity index, unless these trends are extreme. Indeed, there are situations in which it may be interesting to implement a more yielding quantification, which tends to favor false negatives. At the same time, a more strict similarity quantification can be particularly interesting in other situations in which false positives have higher costs and need to be minimized and/or enhance accuracy is expected in the quantification. In summary, the localization of the position of the peak tends to be substantially more robust and accurate in the case of the coincidence than the inner product similarity.

For these reasons, it becomes particularly interesting to consider similarity measurements involving one or more parameters that can be used to control how strict the quantification is, so that this can be adapted to a wide range of situations and applications. Approaches such as *multiresolution* or *multiscale* have been developed with that finality in mind. The present work describes a related approach in which a parameter D is used to control how strict the Jaccard and coincidence similarity indices are.

4 Multiset Similarities in One-Dimensional Spaces

The considered neuronal application of similarity comparison addressed in this work provides an interesting perspective from which to address this issue and its related aspects. More specifically, if we consider that the similarity is to be measured between the synaptic weight y and respective input x, we can simplify the otherwise binary operation as an operation only on x (i.e. a function of x), with y being understood as a parameter. Figure 5 illustrates the real product seen from this perspective, assuming synaptic weight $y = 2$.

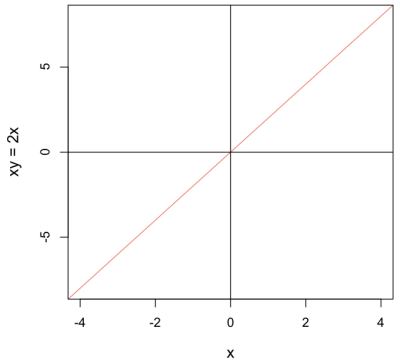

Figure 5: The quantification of similarity between two real values as implemented by the real product xy, with $y = 2$ has severe limitations. The curve should indicate how similar to 2 the values of x are, but monotonically increasing values are obtained instead.

This result well illustrates the limitation of the traditional real product for quantifying similarity. Though the similarity will increase for $|x|$ increasing from 0 to 1, it will continue to increase thereafter. In fact, we have that:

$$\lim_{x \to \infty} xy = \infty \tag{7}$$

with $y = 2$.

As developed in [13], the prototypical function for quantifying similarity in the most strict manner possible consists in the Kronecker delta function, which can be written as:

$$\delta_{x,y} = \begin{cases} 1 & whenever\ x = y \\ 0 & otherwise \end{cases} \tag{8}$$

Though this function cannot provide information about the alignment of the values x and y, it can be readily generalized as:

$$\tilde{\delta}_{x,y} = \begin{cases} 1 & whenever\ x = y \\ -1 & whenever\ x = -y \\ 0 & whenever\ |x| \neq |y| \end{cases} \tag{9}$$

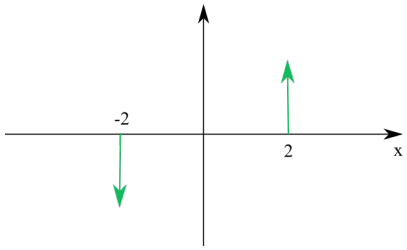

Figure 6: The Kronecker function modified to take into account the relative alignment of the real values x and $y = 2$, which is now reflected in the respective sign.

Figure 6 illustrates this function for $y = 2$, i.e. $\tilde{\delta}_{x,2}$.

The binary Kronecker function generalized to quantify signed similarity is shown in Figure 7.

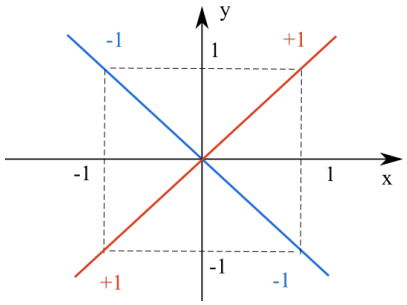

Figure 7: The binary Kronecker function modified to take into account the relative alignment of the real values x and y.

The problem with this generalized Kronecker delta function is that it is simply too strict in its evaluation of the similarity between two real values x and y.

We have from Equation 5 that, when applied on real values x and y in $\mathcal{R}$, the cosine similarity effectively acts as the Kronecker delta function on those two values, therefore presenting rather limited potential for comparing the similarity between x and y.

Interestingly, there is another particularly interesting possibility to quantify the similarity between two real values taking possibly negative values [28, 29, 30, 13]. In particular, the basic scalar version of the operator in [29, 30] follows the same sign rules as the above discussed inner product while involving only the minimum binary operation:

$$x \sqcap y = s_{xy} \min \{s_x x, s_y y\} \tag{10}$$

where $s_x = sign(x)$, $s_y = sign(y)$, and s_{xy} is the *conjoint sign function* $s_{xy} = s_x s_y$.

This operator has also been verified [31, 18, 13] to correspond to the signed intersection between multisets taking real, possibly negative values, being dierctoy related to real-valued adaptations of the Jaccard similarity index.

In particular, it can be understood as a modification of the intersection between two functions in order to consider the common or shared area of the functions with respect to the horizontal axis.

Interestingly, this product has surprising properties, including: (i) it is extremely simple to be implemented [29, 30], e.g. in analog electronic circuits [32]; (ii) it is conceptually simple; (iii) it obeys the sign rules in Equation 3; (iv) its magnitude is bound by the absolute value of the minimum between x and y; (v) unlike the cosine similarity when applied to 1D spaces ($x, y \in \mathcal{R}$), the real-valued Jaccard index is not limited to yielding ± 1 values, but is instead capable of providing a detailed quantification of the respective similarity.

It is therefore interesting to consider this function from the neuronal perspective, i.e. with one of its values kept constant so as to correspond with the respective weights. Figure 8 illustrates the operation $x \sqcap y$ for $y = 2$, which can be understood as being analogous to the 'receptive field' of a respective neuron in the one-dimensional space $\mathcal{R}$.

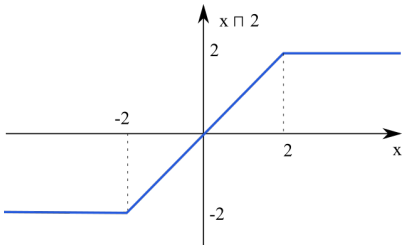

Figure 8: The operation $x \sqcap y$ assuming $y = 2$, i.e. $x \sqcap 2$. Now we have that $-2 \leq x \sqcap 2 \leq 2$ The obtained profile can be understood as being analogous to the 'receptive field' of a respective neuron operating in a one-dimensional input space.

It is now clear that this operation, when one of its argument is kept constant, corresponds to a clipped version of the real product $2x$ as in our previous example. The saturation observed for $x > 2$ is a critical feature in which it implies $x \sqcap y$ to become bound by the fixed value.

However, maximum similarity will be observed for any value of x larger than 2. An interesting manner to circumvent this saturation problem consists of adopting the following normalization:

$$J(x, y) = \frac{s_{xy} \min \{s_x x, s_y y\}}{\max \{s_x x, s_y y\}} = \frac{f \sqcap g}{f \sqcup g} \qquad (11)$$

so that $-1 \leq x \sqcap y \leq 1$.

The above normalized version of the operation $x \sqcap y$ has been verified to correspond to the *real-valued Jaccard index* applied to two real scalar values [13, 18, 14]. As with the product, cosine similarity and Eucliden distance, the Jaccard index is commutative with respect to the two compared values, a propriety that extends to any dimension of the feature space.

Observe that, as with the standard Jaccard similarity index, the respective multiset version above capable of operation on real values is not defined for the comparison between two null sets or feature vectors, as it diverges to $0/0$.

Figure 9 illustrates both the function $n(x, y) = \max \{s_x x, s_y y\}$ and the resulting real-valued Jaccard index.

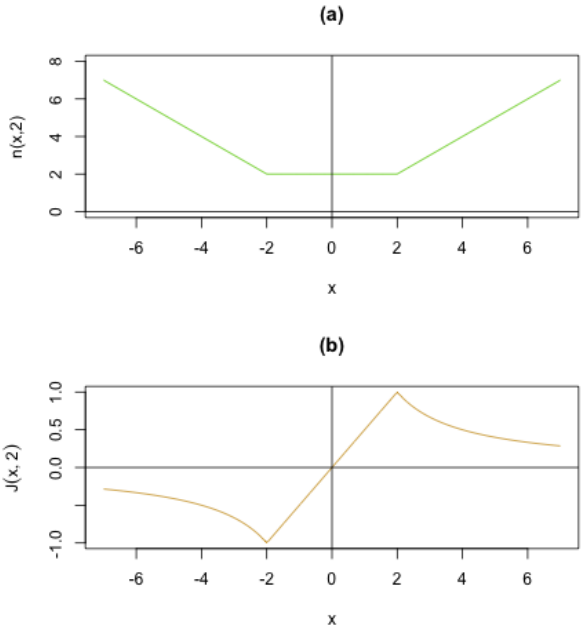

Figure 9: The normalizing function $n(x, 2) = \max \{s_x x, 2\}$ and the normalized operator which corresponds to the real-valued Jaccard index $J(x, 2)$ applied to real scalar values.

The normalizing function that constitutes the denominator has a direct correspondence with the generalized multiset concept of absolute union [31]. Observe that this function increases linearly with x. As a consequence, the division by the normalizing function will penalize the similarities for $|x| > 2$, yielding to two respective peaks in the real-valued Jaccard index $J_R(x, 2)$, providing enhanced quantification selectivity. Interestingly, this resulting index can therefore be understood as a less strict version of the generalized Kronecker delta (compare Figs. 6 and 9b), while being also more strict than the real product (as a consequence of the saturation).

The developments presented above make it clear that it is possible to define an infinity of other similarity indices. For instance, it is possible to control the sharpness of the similarity peaks by using other products and normalizing functions.

As an example, if even sharper peaks are required, we can make:

$$J_3(x, y) = J(x, y)^3 \tag{12}$$

Figure 10 illustrates this function for $y = 2$.

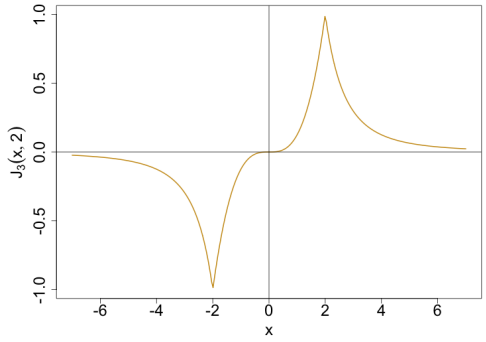

Figure 10: The similarity function $J_3(x, 2)$, when compared to the real-valued Jaccard index, is characterized by a sharper peak, therefore implying even more strict similarity quantification.

The above development can be generalized to any non-negative integer degree D odd as:

$$J_D(x, y) = J(x, y)^D \tag{13}$$

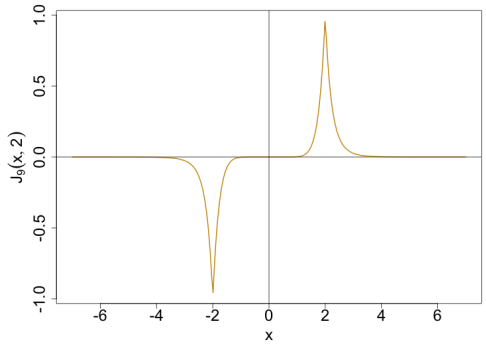

Figure 11: Similarity quantification through the function $S_{D=9}(x, 2)$.

An adaptation can be also implemented in case we need to consider D even. It is also possible to have less strict similarity comparison by adopting $D < 1$, which also requires some adaptation of Equation 13.

Observe that the similarity function $S_D(x, y)$ tends to the generalized Kronecker delta function when $D \to \infty$, D odd, i.e.:

$$\lim_{D\to\infty} S_D(x, y) = \tilde{\delta}(x, y) \tag{14}$$

However, for simplicity's sake, we will consider only the real-valued Jaccard index in our subsequent performance analysis, which can be understood as the above construction when $D = 0$. A more systematic study of higher values of D will be reported opportunely.

Given that the Jaccard similarity index has been verified not to be able to take into account the relative interiority (or overlap, e.g. [33]) between the two compared vectors, the *coincidence similarity* has been proposed as a respective complementation, consisting of the product between the real-valued Jaccard and interiority indices:

$$\mathcal{C}_R(\vec{x}, \vec{y}) = \mathcal{J}_R(\vec{x}, \vec{y})\ \mathcal{I}_R(\vec{x}, \vec{y}) \tag{15}$$

Since the coincidence index does not distinguish from the respective real-valued Jaccard index for the one-dimensional input (i.e. $x, y, \in \mathcal{R}$), we now assume that the two values to be compared are vectors in an $N-$dimensional space, i.e. $\vec{x}, \vec{y} \in \mathcal{R}^N$.

In this case, the real-valued Jaccard index can be expressed as:

$$\mathcal{J}_R(\vec{x}, \vec{y}) = \frac{\sum_{i=1}^{N} s_{x_i y_i} \min\{s_{x_i} x_i, s_{y_i} y_i\}}{\sum_{i=1}^{N} \max\{s_{x_i} x_i, s_{y_i} y_i\}} \tag{16}$$

The interiority index for real valued vectors can be expressed [13, 14, 18] as:

$$I(\vec{x}, \vec{y}) = \frac{\sum_{i=1}^{N} \min\{s_{x_i} x_i, s_{y_i} y_i\}}{\max\{S_{\vec{x}}, S_{\vec{y}}\}} \tag{17}$$

where:

$$S_{\vec{x}} = \sum_{i=1}^{N} s_{x_i} x_i \tag{18}$$

$$S_{\vec{y}} = \sum_{i=1}^{N} s_{y_i} y_i \tag{19}$$

It is interesting to observe that both the Jaccard and interiority indices, as with the Euclidean distance, are *invariant to permutations* of the indexing i of the input components, in the sense that any changes in the order of the two input vectors will yield identical results. The permutation invariance of similarity or distance indices, which implies that they cannot take into account the sense of eventual input rotations or reflections, is compatible with the fact that the order of the features in pattern recognition systems can rarely be specified.

5 Multiset Similarities in Two-Dimensional Spaces

Having presented and discussed the properties of the inner product and real-valued Jaccard similarity indices respectively to comparing two real values x and y, we now

extend that discussion to two dimensional spaces, so that now we are interested in comparing the similarity between two real-valued vectors $\vec{x} = [x_1, y_1]^T$ and $\vec{y} == [x_2, y_2]^T$, with $\vec{x}, \vec{y} \in \mathcal{R}^2$.

Figure 12 presents the cosine similarity calculated between a reference vector $\vec{y} = [1, 2]^T$ and vectors $\vec{x} = [x_1, y_1]^T$ with $4 \leq x_1, y_1 \leq 4$.

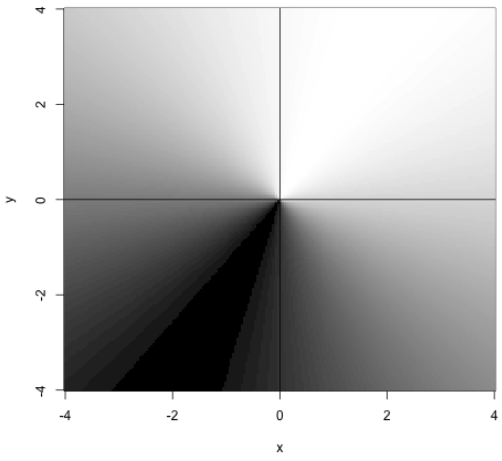

Figure 12: Cosine similarity values (shown in grayscale from dark to bright) obtained for the cosine similarity index between a reference vector $\vec{y} = [1, 2]^T$ and vectors $\vec{x} = [x_1, y_1]^T$ with $4 \leq x_1, y_1 \leq 4$.

The maximum similarity takes place for the angle sector containing the vector $\vec{y}$, but any other vector with the same angle will imply identical cosine similarity, therefore illustrating the fact that the cosine similarity cannot distinguish between any two vectors with the same orientation but distinct magnitudes. In addition, observe that the gray levels undergo rather little variations for vectors with orientations similar to that of $\vec{y} = [1, 2]^T$. These issues can have severe impact on the pattern recognition performance of individual neurons based on the cosine similarity. Analogous implications are expected for $N-$dimensional input.

Figure 13 depicts the similarity values obtained for the real-valued Jaccard index considering the same comparison problem as before. The surface in this and the subsequent figures in this section are shown with substantially reduced gray level resolution (comparatively to that in Fig. 12) in order to make the underlying geometry of the surfaces more discernible in terms of respective level set curves.

Unlike the results obtained for the cosine similarity, now we have a well-defined and delimited peak (bright gray levels) corresponding to the position $\vec{y} = [1, 2]^T$.

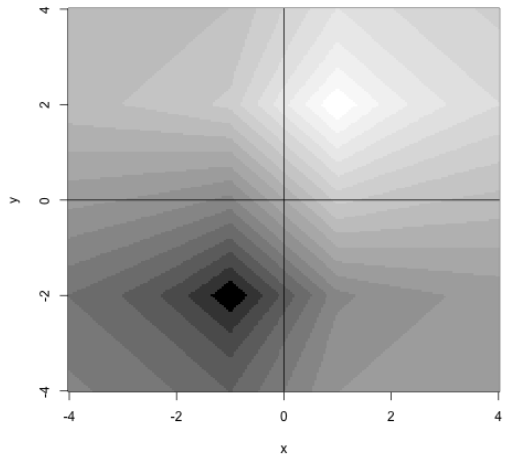

Figure 13: Jaccard similarity values ($D = 1$) obtained when comparing two real-valued vectors $\vec{x} = [x_1, y_1]^T$ and $\vec{y} = [1, 2]^T$, with $4 \leq x_1, y_1 \leq 4$.

As expected, a minimum peak is also observed at $\vec{y} = [-1, -2]^T$. The enhanced specificity and strictness of the comparison implemented by the real-valued Jaccard index, when compared to the cosine similarity results in Figure 12, are striking. As in the one-dimensional case discussed in the previous section, the real-valued Jaccard similarity index has been able to quantify the input similarity with great accuracy while preserving a good level of generalization.

The Jaccard similarity presents an intrinsic geometry and symmetry worth focusing attention on. Figure 14 depicts a diagram of the equisimilarity region defined by making $\mathcal{J}_R(\vec{x}, \vec{y})$ equal to a constant value d.

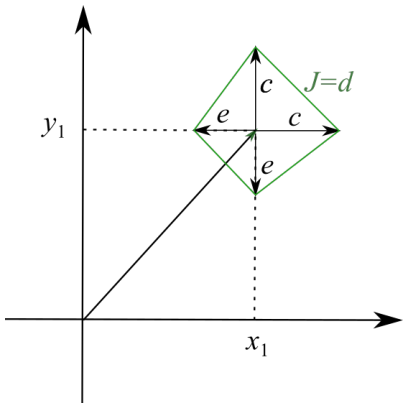

Figure 14: The basic construction characterizing the equisimilarity region for the real-valued Jaccard, defined by the position of vectors $\vec{v_2} = [x2, y2]^T$ when compared to a reference vector $\vec{v_1} = [x1, y1]^T$ and fixed Jaccard similarity value $J = d$.

While keeping x_1 fixed, and assuming $y_2 > y_1$, we can write:

$$d = \mathcal{J}(\vec{v_1}, \vec{v_2}) = \frac{y_1 + y_2}{y_1 + y_2 + d} = \frac{y_1 + y_2 - e}{y_1 + y_2} \tag{20}$$

which implies:

$$c = \frac{(y_1 + y_2)(1 - d)}{d} \tag{21}$$

$$e = (y_1 + y_2)(1 - d) \tag{22}$$

It also follows that:

$$d = \frac{e}{c} \tag{23}$$

meaning that the equisimilarity regions tends to a symmetric diamond when $d \to 1$.

Now, if we scale both vectors as $\vec{v}_{1,s} = \kappa\vec{v}_2$ and $\vec{v}_{2,s} = \kappa\vec{v}_2$, with $\kappa \in \mathcal{R}$, it follows that the dimensions of the respectively scaled region are $c_s = \kappa c$ and $e_s = \kappa e$, indicating that the size of the equisimilarity region changes linearly with the scaling of the vectors being compared.

In other words, the real-valued Jaccard similarity naturally implements the often sought scaling invariance, being normalized respectively to the magnitude of the vectors. This is in contrast to the Euclidean distance, which has constant equisimilarity region, so that normalization with respect to scale requires additional calculations of vector magnitudes and respective divisions. Thus, the Jaccard similarity values are relative to the vectors magnitude. Figure 15 illustrates several equisimilarity regions for the real-values Jaccard similarity. An analogous property characterizes the coincidence similarity index, as it derives directly from the Jaccard index.

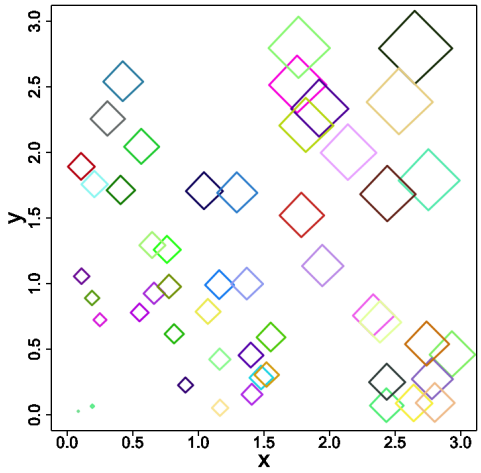

Figure 15: The real-valued Jaccard similarity index is naturally normalized with respect to the scaling of the magnitudes of the compared vectors. This figure illustrates several equisimilarity regions obtained for the real-valued Jaccard similarity with $J = d = 0.95$. Observe the linear scale of the regions size with the position of the reference vector.

Figure 16 presents the coincidence similarity values obtained for the same comparison problem. An even more strict comparison can be obtained. Observe also, in comparison with the surface in Figure 13, the distinct shape of the level-set contours, which reflect the incorporation of the interiority index into the Jaccard similarity quantification.

Even stricter, sharper comparisons can be obtained by using $D > 1$. Figure 17 presents the similarity surface obtained for the real-valued Jaccard index with $D = 9$. Substantially sharper peaks are obtained at the expense of reduced generalization capabaility.

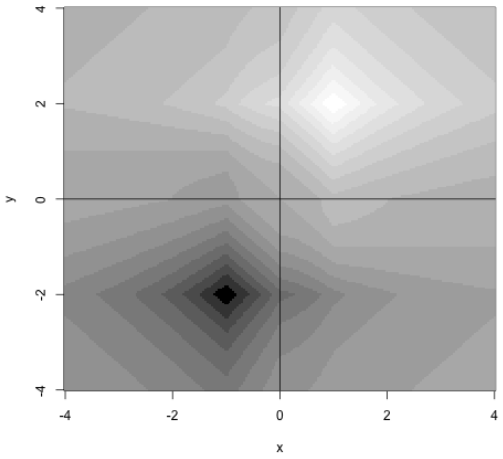

Figure 16: The coincidence similarity obtained while comparing two real-valued vectors $\vec{v}_1 = [x_1, y_1]^T$ and $\vec{v}_2 = [1, 2]^T$, with $4 \leq x_1, y_1 \leq 4$.

As described in [15], both the real-valued Jaccard and real-valued coincidence indices can be generalized to incorporate a parameter α, $0 \leq \alpha \leq 1$, controlling the relative contribution of the pairwise features with the same or opposite signs on the resulting similarity values. In case $\alpha > 0.5$, the contribution of the pairwise features with the same sign will be enhanced, with the opposite taking place for α. When $\alpha = 0.5$, this index becomes identical to its parameterless version. The availability of the parameter α has been verified to enhance the level of details and modularity when of the application of the coincidence for translating datasets described by respective features into complex networks (e.g. [15]).

Figures 18 and Figures 19 presents the coincidence values obtained for the same comparison problem as above, but with $\alpha = 0.7$ and $\alpha = 0.3$, respectively.

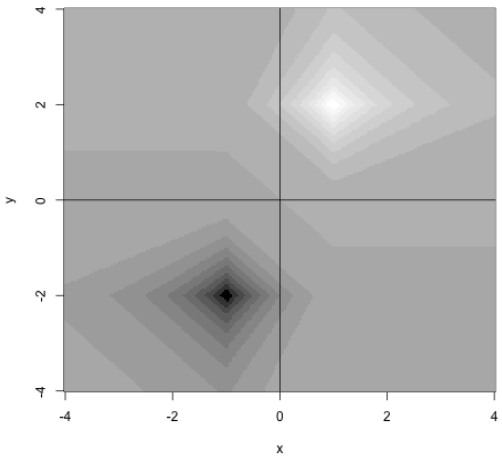

Figure 17: The Jaccard similarity obtained for $D = 9$ while comparing two real-valued vectors $\vec{v}_1 = [x_1, y_1]^T$ and $\vec{v}_2 = [1, 2]^T$, with $4 \leq x_1, x_2 \leq 4$.

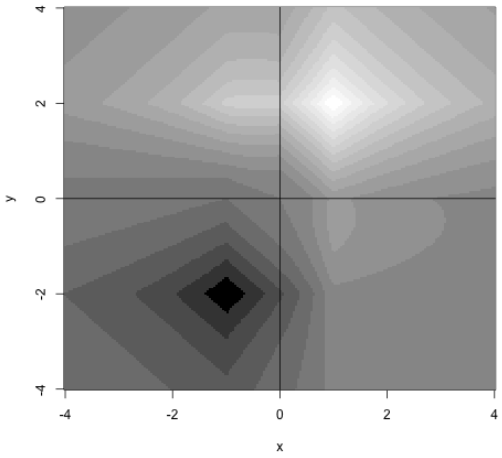

Figure 18: The coincidence similarity obtained for $D = 1$ with $\alpha = 0.7$ while comparing two real-valued vectors $\vec{v}_1 = [x_1, y_1]^T$ and $\vec{v}_2 = [1, 2]^T$, with $4 \leq x_1, y_1 \leq 4$. The maximum and minimum obtained coincidence values are 0.691 and -0.296, respectively, confirming the enhancement of the contribution of pairwise features with the same sign.

The effect of emphasizing the relevance of pairwise features have the same or opposite signs is marked in these figures, confirming the importance of the additional parameter α in controlling how aligned or anti-aligned pairs of features are taking into account, which can lead to enhanced comparison details. Observe also that the adoption of $\alpha \neq 0.5$ implies in the positive and negative peaks to become asymmetric, with the peak with the lower magnitude becoming smaller and less sharp.

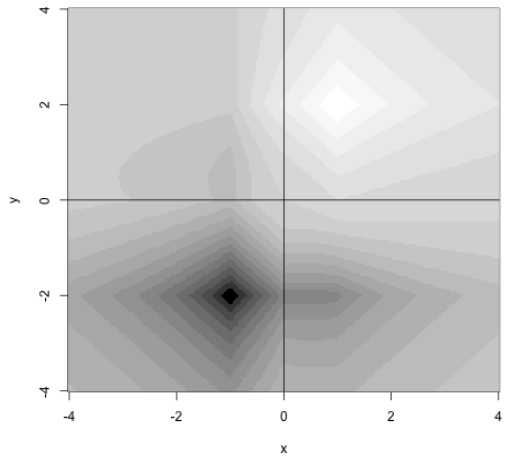

Figure 19: The coincidence similarity obtained for $D = 1$ with $\alpha = 0.3$ while comparing two real-valued vectors $\vec{v}_1 = [x_1, y_1]^T$ and $\vec{v}_2 = [1, 2]^T$, with $4 \leq x_1, y_1 \leq 4$. The maximum and minimum obtained coincidence values are 0.296 and -0.691, respectively, confirming the enhancement of the contribution of pairwise features with the same sign.

6 Membership Interpretation of Multiset Similarity

One additional interesting characteristic of multiset-based similarity approaches, as with the Jaccard and coincidence indices, consists in that a powerful intuition regarding the basis of the similarity quantification can be obtained in terms of the the concept of membership and respective graphical representations. This important aspect is addressed in the present section. For simplicity's sake, we will be constrained to the case in which all values to be compared are non-negative. The extension to real values can be obtained by using the real-valued versions of these two multiset similarity indices [14, 13].

We start by going back to the definition of the traditional Jaccard index, as in Equation 1. Here, we have to set operations, namely *union* and *intersection*. It is of particular interest to observe that this classic definition of the Jaccard index therefore relies on the relevant concept of *membership* between elements to the respectively compared sets.

In multiset theory (e.g. [18]), the repetition of elements in multisets is allowed, leading to the concept of *multiplicity* of each element. Thus, a multiset A can be represented in terms of ordered pairs $[a, m_a]$, where a is the elements identifier, which can be categorical or numeric, while n_a quantifies how many entries of element a are found in the multiset A. For instance, a multiset A containing three apples, two pears and five oranges can be represented as:

$$A = \{[apple, 3], [pear, 2], [orange, 5]\} \quad (24)$$

The set of all possible elements is often called the *support* of the respective multiset. In the previous example we would have $S_A = \{apple, pear, orange\}$.

As discussed in [14, 13], real-valued functions of the type $f(x)$ can be immediately mapped into a multisets with an infinite number of elements by understanding the element identifiers x_i as the abscissa value, while the function value $f(x_i)$ at that element is mapped into the respective multiplicity, i.e.:

$$f = \{[x_1, m_{x_1} = f(x_1)], [x_2, m_{x_2} = f(x_2)], \ldots]\} \quad (25)$$

For simplicity's sake, in the present work we restrict our attention to samples of N values of the function, therefore yielding discrete functions (which can be represented as vectors), and non-negative values of multiplicity.

The multiset operations of union and intersection between two functions f and g with a shared support S can now be defined as:

$$f \cup g = \\ = \{[x_1, \max\{f(x_1), g(x_1)\}], [x_2, \max\{f(x_2), g(x_2)\}], \ldots\} \quad (26)$$

$$f \cap g = \\ = \{[x_1, \min\{f(x_1), g(x_1)\}], [x_2, \min\{f(x_2), g(x_2)\}], \ldots\} \quad (27)$$

The Jaccard similarity index can now be defined as:

$$\mathcal{J}(f, g) = \frac{\sum_{i=1}^{N} \min\{f(x_i), g(x_i)\}}{\sum_{i=1}^{N} \max\{f(x_i), g(x_i)\}} \quad (28)$$

Now, it happens that these two operations have a powerful intuitive geometrical interpretation in terms of the visualization of the two functions and their respective areas. Consider the situation depicted in Figure 20, presenting two discrete functions $f(x_i)$ and $g(x_i)$, with x_i equally spaced along the function domain x.

The sum of the values $\sum_{i=1}^{N} \min\{f(x_i), g(x_i)\}$ can be immediately understood as being proportional to the area of the function $f(x)$ along the N samples support. Interestingly, this interpretation does not require any adjacency or order relationship between the coordinates x_i, because the are under the function is *invariant to permutations* of those elements. A similar interpretation readily holds for the union multiset operation.

Now, the numerator in Equation 28 can be associated to being proportional to the area below the minimum between the two function values, corresponding to the area *shared* by the two functions, while the denominator is proportional to the area defined by the maximum values between the two functions ordinates, which can be understood as the *outline* of the two functions.

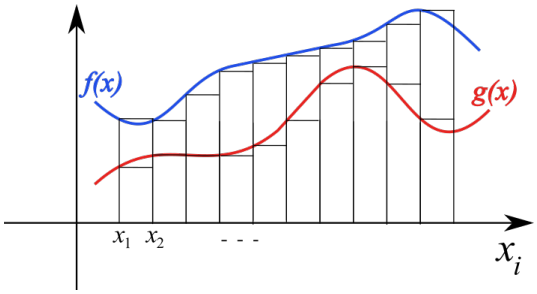

Figure 20: Two functions $f(x)$ and $g(x)$ sampled at equally spaced x_i abscissa values. These two discrete functions can be exactly represented as respective multisets. For simplicity's sake it is assumed that $f(x) \geq 0$ and $g(x) \geq 0$. The common (or shared) area between these two functions is proportional to the *multiset intersection* between them. The area of the outline of the two functions (maximum values between them) is proportional to the *multiset union* (e.g. [14, 13]). Though the two functions may intersect one another at several points, for simplicity's sake this is not illustrated in this figure.

The above developments means that the Jaccard index as defined in Equation 28 can now be conceptually understood as corresponding to the ratio between the area shared by the the two functions and the area of the functions outline. Thus, when $f(x) = g(x)$, we have that the shared and outline areas are identical, leading to $\mathcal{J}(f, g) = 1$. When any of the two functions is null, we have $\mathcal{J}(f, g) = 1$. As with the traditional Jaccard index, the result is not defined when both input functions are null. When $f(x)$ and $g(x)$ are similar, the shared and outline areas will be similar, leading to high Jaccard values. However, if $f(x)$ and $g(x)$ are different, small values will be respectively obtained.

The interiority index can also be understood in an manner analogous to the Jaccard index as developed above. More specifically, it corresponds to the area of the shared region divided by the smallest area between the two functions. For instance, the situation shown in Figure **??** is characterized by having interiority index equal to 1 because one of the functions is contained completely within the other. The coincidence index can then be immediately understood as corresponding to the product of the Jaccard and interiority indices.

The interesting geometrical interpretation of the Jaccard index developed above provides a particularly valuable resource for better understanding and applying both the multiset Jaccard and multiset coincidence similarities. One of the most important implications of the above developed interpretations of the Jaccard and coincidence indices is that the obtained similarity values can be understood as depending on ratios between areas, being there-

fore completely independent of geometrical transformations such as rotation as is the case, for instance, of the Euclidean distance. Instead, those two indices are directly related not to the concept of *distances*, but to the also important notion of *membership* of each element respectively to the two multisets. As such, the obtained similarity quantifications related to how much the two functions coincide geometrically (permutation invariant), and not to formal metrics such as the Euclidean distance.

In the case of the Euclidean distance, even if its values are permutation invariant, the respective translational and rotational invariance usually is almost never verified in typical feature spaces, as discussed in Section 2. At the same time, it is interesting to realize that the vectors that are equidistant (in the Euclidean sense) from a given a reference function (template) actually imply non-equivalent multiset similarities, therefore implying distinct relative membership relationships between the compared vectors (or functions, or multisets). All in all, the relative membership property does not rely on having the adopted features to correspond to an orthonormal system of coordinates, while the interpretation of equidistance and rotation does.

In summary, a good deal of the effectiveness of the Jaccard and coincidence similarities ultimately stems from being based on relative membership quantifications that are effectively appreciated in terms of the conceptual interpretations in terms of areas of functions as developed in this section.

7 Sensitivity to Localized Perturbations

When dealing with the features to be input to a pattern recognition system such as a neuronal cell, standardization of each of the individual features along its ensemble is often adopted as a means to normalize the dispersion of each feature so it has null mean and unit standard deviation. This is implemented in order to avoid that features taking larger or shifted values predominate over the other features with smaller magnitude. In other words, every effort is often made so that no individual feature dominate the results.

This same concern extends naturally to the effect of variations of any of the features magnitude on the overall result. That is important in cases such in which some of the features are too noisy or not particularly relevant, which is often the case.

This section addresses the sensitivity of the Jaccard and cosine similarities, as well as the normalized Euclidean distance with respect to small perturbations to any of the isolated components of the two vectors to be compared.

We focus on the situation in whch all x_i, y_i are positive, with $y_i > x_i$, $\forall i$, but the results are similar for the other cases. In this case, the Jaccard similarity can be simplified as:

$$\mathcal{J}_R(\vec{x},\vec{y}) = \frac{\sum_{i=1}^{N} x_i}{\sum_{i=1}^{N} y_i} \tag{29}$$

so that the respective variation implied by the small perturbation ∂x_i can be immediately obtained as:

$$\frac{\partial \mathcal{J}_R(\vec{x},\vec{y})}{\partial x_i} = \frac{1}{\sum_{i=1}^{N} y_i} \tag{30}$$

From the definition of Euclidian distance, we have:

$$E(\vec{x},\vec{y}) = 2\sqrt{\sum_{i=1}^{N} (x_i - y_i)^2} \tag{31}$$

When normalized by the average of the magnitudes of $\vec{x}$ and $\vec{y}$, this distance becomes:

$$E(\vec{x},\vec{y}) = 2\frac{\sqrt{\sum_{i=1}^{N} (x_i - y_i)^2}}{||\vec{x}|| + ||\vec{y}||} \tag{32}$$

Assuming that the variation ∂x_1 does not significantly change $||\vec{x}||$, we can derive the following approximation:

$$\frac{\partial E(\vec{x},\vec{y})}{\partial x_i} \approx \frac{x_i - y_i}{||\vec{x}|| + ||\vec{y}||} \tag{33}$$

from which we can infer that small perturbations to any individual component x_i will imply variations of the normalized Euclidean distance that are not only proportional to the magnitude of x_i, but also depend strongly on y_i. Of particular relevance is the fact that, for a specific component i, when x_i is similar to y_i, small perturbations of the former will have little effect on the distance variations, indicating that the contribution of that specific features to the resulting distance is small when the compared data are similar. However, when the two values x_i and y_i are markedly different, the localize perturbations will have stronger effect on the result. This implies that perturbations (error or noise) in components that are substantially different between the two compared vectors can have pronounced effect on the resulting distance. This situation is completely different from that observed for the Jaccard similarity, as the localized perturbations will all have the same influence on the resulting similarity value irrespectively to the values of x_i and y_i.

Figure 21 illustrates the relative variations of the normalized Euclidean distance, as well as Jaccard and cosine similarities in terms of the magnitude of small perturbations to a single component, assuming $N = 100$, each of the components of $\vec{x}$ drawn from a normal distribution with average 10 and standard deviation 3, and $\vec{y}$ obtained

by adding $\vec{x}$ to 0.1 multiplied by a vector with coordinates drawn from a normal distribution with mean 1 and standard deviation 5. The values were obtained from 10000 random experiments.

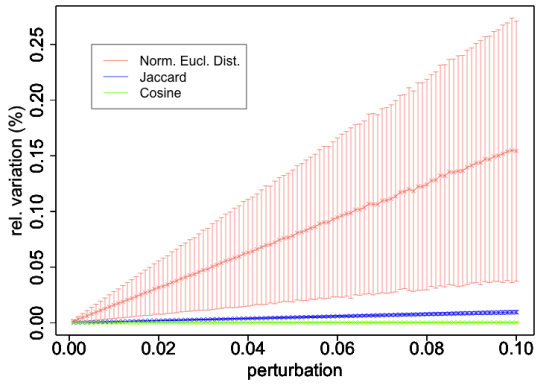

Figure 21: Relative variations of the Jaccard and cosine similarities, as well as the normalized Euclidean distance, to small perturbations of a single component x_i of one of the vectors being compared. Values are shown as average $\pm$ standard deviation, in terms of the magnitude of the individual perturbations. The stabilities of the two similarities, regarding both the average and standard deviations of the relative variations, are substantially smaller than that of the normalized Euclidean distance.

Though respective to a specific configuration, these results still illustrate that the normalized Euclidean distance is particularly sensitive to small perturbations on the magnitude of any of the components of the vectors being compared. This often represents a substantial shortcoming while comparing vectors and recognizing patterns, especially with some of the components are particularly noisy or not so much relevant to the pattern analysis.

Given that the sensitivity of the coincidence similarity can be verified to be comparable to that of the Jaccard similarity, and considering that the cosine similarity implements little strict comparisons, we have that the Jaccard and coincidence similarities tend to have substantial advantages regarding the stability of the obtained results respectively to perturbations implied by some of the components of the vectors being compared.

8 Generalized Multiset Neurons

Traditional implementations of artificial neuronal networks, as integrate-and-fire models as McCulloch and Pitts and perceptrons (e.g. [1, 2]), often involve the inner product of the input signal with the respective synaptic weights (bilinear operation) followed by a non-linearity output function. As such, these neurons implement linear discrimination.

The multiscale neurons described so far in the present work involve a comparison between two vectors, one of which can be understood as a template, while the other corresponds to the input signal to be compared with the template. We have seen in the previous section that these neurons have 2D receptive fields that resemble diamonds. In addition to being able to compare generic templates in any dimension, it is also possible to use this type of neuron to implement binary decision regions. This can be accomplished by incorporating a non-linear output function, as in the integrate-and-fire paradigm that receives the Jaccard value as input, while the output intensity can be understood as an indication of the certainty of the template recognition.

The hard limit and sigmoid functions are frequently adopted for implementing the output stage of neuronal cells. There are several types of sigmoid functions, but in this work we adopt the following definition:

$$f(x) = \frac{1}{1 + e^{-(a(x-T))}} \tag{34}$$

where a controls the sharpness of the transition from 0 to 1 and T specifies the value of x where the transition takes place.

Figure 22(a) illustrates one neuron of this type (Jaccard similarity) considering $N-$dimensional input, while some possible $2-$dimensional decision regions illustrated in (b).

Interestingly, each real-valued Jaccard or coincidence neuron on 2D inputs spaces can be understood as implementing four linear discriminations, corresponding to each of the sides of the respective diamond decision region, which means that each of these types of neurons effectively corresponds to four more traditional linear discriminant neurons based on the inner product and hard limit output function.

Another interesting possibility is to connect the output from multiset neurons to other multiset neurons, therefore defining multilayer neuronal multiset networks.

Though it may firstly appear that the multiset neurons implement more specific decision regions, they are in fact much more generic and versatile than integrate-and-fire neurons. In order to harness the full potential of multiset neurons, it is necessary to incorporate a small modification in the sense that each synaptic input is multiplied by a respective weight, as illustrated in Figure 23, while a possible respective decision region is exemplified in Figure 24. This decision region corresponds to the product of two decision regions of two individual geminis with hard limit output, followed by a pointwise product (or logical and). Five neurons of the integrate-and-fire traditional type would be otherwise required for implementing this type of decision region. Much more general and versatile

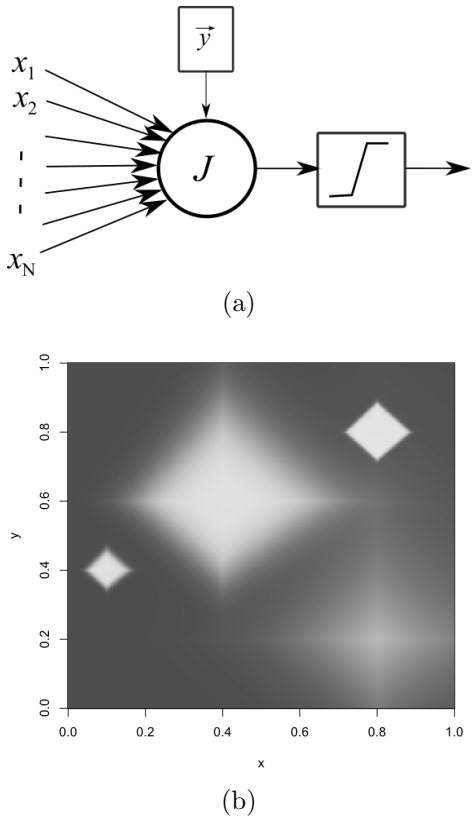

Figure 22: A generalized multiset neuron with N inputs incorporating a non-linear hardlimiting output function, and examples of single neuron 2D receptive fields (b) obtained by varying the sigmoid parameters and template coordinates.

combinations of decision regions can be obtained in analogue manner. These neurons are henceforth referred to as *generalized multiset neurons*, or *geminis* (GMNs) for short.

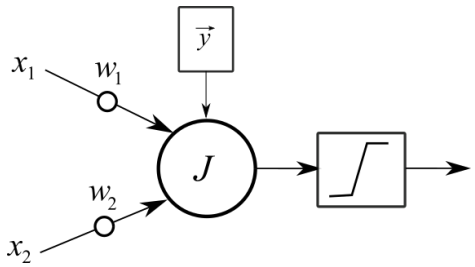

Figure 23: The *gemini* neuron. The generalization of multiset neurons to incorporate non-linear output function as well as synaptic weights associated to each of its inputs. The comparison part of the neuron can be based on the real-valued Jaccard or coincidence similarities with generic parameter configurations.

The fact that the basic decision region of a multiset neuron is a diamond, while a half-plan is obtained for integrate-and-fire neurons, allows impressive possibilities

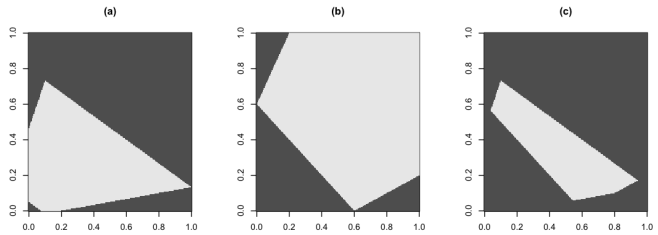

Figure 24: The decision regions (a,b) of two gemini neurons with hard-limit outputs are multiplied in pointwise manner yielding an elaborate decision region which would otherwise require at least 5 more traditional linear discriminant integrate-and-fire neuronal cells.

for obtained quite elaborate and generic decision regions by combining the input from just a few geminis.

9 Single Neuron Comparison

In this section, we perform a comparison of single neurons defined respectively to the real-valued Jaccard, interiority, and coincidence indices, as well as to the classic inner product. The similarity indices are considered for implementing the synaptic efficiency and dendritic integration of stimuli up to the implantation cone. Therefore, the intrinsic non-linearity of the latter is not considered in this work. The non-linearity here is accounted by the multiset-based operations implemented at each synapsis.

This comparison is developed by taking into account several possible effects commonly found regarding pattern recognition by single neuronal cells, including: (a) relative position displacements; (b) stimulus size variation (scaling); (c) stimulus intensity variation; (d) noise; and (e) presence of more than a single pattern in the stimulus.

The reference input stimulus will be a circularly symmetry two-dimensional gaussian function centered at the stimulus space, given as:

$$g(x,y) = e^{-0.5\left(\frac{d(x,y)}{\sigma}\right)^2} \tag{35}$$

$$\textit{where: } d(x,y) = \sqrt{x^2+y^2} \tag{36}$$

Unless otherwise stated, we adopt $\sigma = 100$ in an 200×200 image support.

Figure 25 presents the values of the four considered methods respective to relative displacements from 0 to 30 discrete steps (pixels). Full similarity has been duly identified by all methods regarding null displacement, as could be expected. However, as soon as one of the patterns shifts, the values of all indices are decreased. The sharpest decrease is verified for the coincidence approach, which is known [14, 13] to provide a more strict quantification of pairwise similarity.

The classic cross correlation presented the slowest decrease between all methods, except for displacements above 12 pixes, in which case all the indices values are already very small. This is in agreement with the identification of product based similarities [14, 13] to be particularly tolerant to pairwise differences. The real-valued Jaccard approach yielded the second fastest decreasing values.

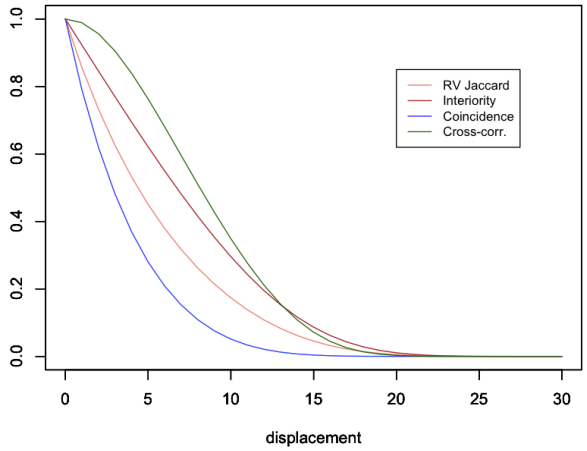

Figure 25: Similarity values obtained by the four considered methods respectively to relative displacements of two identical gaussians. The coincidence method allowed the fastest, and therefore most strict, quantification of the similarity, while the classic cross correlation yielded the most tolerant and least discriminative results.

Next, we analyze the similarity quantification in terms of varying intensities of one of the two identical gaussians, though one of them was displaced by 2 pixels along both axes in order to impose a more challenging similarity quantification. The considered intensity changes varied in a range from 0 to 3. The results are depicted in Figure 26.

Particularly interesting results can be discerned from this figure. Of greatest notice is the complete insensitivity of the classic cross-correlation method to the intensity variations. Though this feature can be helpful in some applications where intensity variance is desired, it will completely fail in cases where more strict quantifications of similarity are required to take into account also the relative intensities. The best results in this sense have been obtained with respect to the coincidence methodology, followed by the real-valued Jaccard approach. The interiority yielded a counter intuitive result, in the sense that it presented the smallest value precisely when the two compared patterns have the same intensity. That is so because of the 2 pixels displacements along the two axes.

It is also worth noticing that the two multiset-based

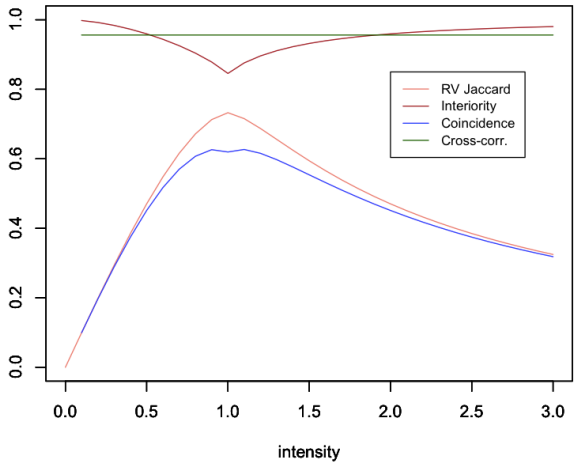

Figure 26: Quantification of the similarity between two circularly symmetric gaussians with the same dispersion, but one of them multiplied by a scaling factor from 0 to 3. In order to impose a more challenging demand, one of the gaussians was always shifted by 2 pixels along each axis. The best results are again observed for the coincidence method, followed by the real-valued Jaccard and interiority approaches. The classic cross correlated revealed to be completely insensitive to the intensity changes.

methodologies present two main behaviors. From intensities ranging from 0 to 1, meaning that one of the patterns is less intense than the reference, both these methods present an almost linear increase up to identical intensity. The maximum similarity value 1 was not obtained in this case because of the small imposed relative displacement of 2 pixels along each axes. From this peak, the similarity values then decrease progressively as the intensities, which now correspond to magnifications, increase.

The results of the study of the effect of the pattern width (or scaling) on the respective matching is shown in Figure 27. The width, which corresponded to the standard deviation of the circularly symmetric gaussian, given in Equation 35, varied from 0 to 100.

Both the real-valued Jaccard and the coincidence match values presented a linear increase from 0 to 1. Recall that, in this experiment, both compared patterns correspond to circularly symmetric gaussians with $\sigma = 100$ pixels.

The classic cross-correlation presented an initially steep increasing profile followed by a saturation. As expected, the interiority index was kept constant with value 1, reflecting the fact that one of the patterns is always interior to the other in this particular experiment. The real-valued Jaccard and coincidence indices represent a suitable choice in case the similarity is to reflect the width discrepancy in a linear manner. The classic cross correlation again resulted more tolerant to the implemented variation, reaching relatively high values sooner than the

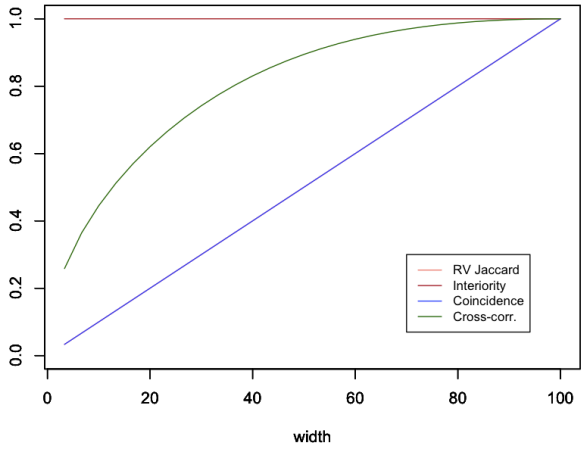

Figure 27: The similarity between the two patterns in terms of the variation of the width, corresponding to the standard deviation, of one of them. The similarity for the real-time Jaccard and coincidence approaches varies linearly from 0 to 1. The cross correlation presents a steep initial variation followed by a saturation. The kept constant at 1, which is expected given that one of the patterns is always interior to the other.

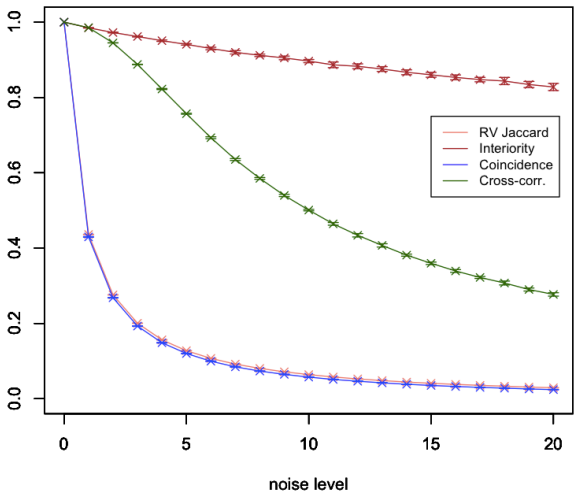

Figure 28: Similarity values obtained by the four considered methods respectively to increasing noise levels. The interiority approach is the most tolerant, followed by the classic cross-correlation, and then the two multiset-based methods. Though these curves correspond to respective averages ± standard deviations, the latter are generally very small to be visualized.

multiset-based methods.

We now proceed to the consideration of additive symmetric uniform noise to one of the patterns. More specifically, the following noise levels are added:

$$X\,[x,y] = X\,[x,y] + \frac{i}{N_{ns}}\,[u(x,y) - 0.5] \qquad (37)$$

with $i = 0, 1, \ldots, N_{ns}$ and where $u(x,y)$ is a scalar uniform random field taking values in $[0.1]$. We henceforth adopt $N_{ns} = 20$. A total of 20 experiments were performed for each of these levels, the respective average and standard deviation being then considered as results.

Figure 28 illustrates the similarity values obtained by the four methods with respect to increasing levels of noise. Several aspects of interest can be identified from this figure. First, we have that the interiority similarity accounts for the slowest decreasing similarity values. This can be explained by the fact that the noisy versions of one of the patterns, despite being jagged, will be mostly interior to the other.

The fastest decreasing profiles are those obtained for the real-valued Jaccard and coincidence methods, which also resulted very similar one another. This indicates that these two multiset-based approaches are the most sensitive to the pattern modifications induced by the increasing levels of noise. The classic cross-correlation yielded an intermediate result between the interiority and multiset-based methods, again reflecting its increase tolerance to perturbations.

The last considered type of perturbation concerns the signed addition of whole gaussian patterns into one of the images. From 1 to 5 such patterns have been added into one of the images at uniformly random positions. The patterns can be added while being multiplied by $+1$ or -1, chosen in uniformly random manner. The results are shown in Figure 29.

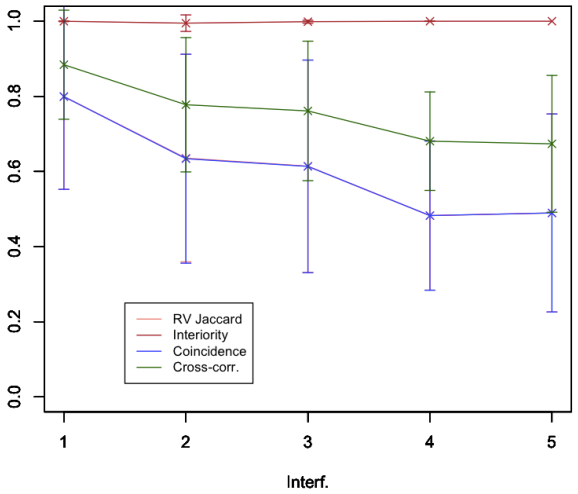

Figure 29: Similarity values obtained in presence of added interference corresponding to signed addition of from 1 to 5 gaussian patterns at uniformly random positions in the image. The curves correspond to the average ± standard deviations. Identical results have been obtained for the real-valued Jaccard and coincidence based similarities.

While the interiority and classic cross-correlation presented total tolerance to the added interference, a mod-

erate discrimination can be observed in the case of the real-valued Jaccard and coincidence results, which present total overlap in the figure.

All in all, the several analysis reported in this section further substantiated the tendency of the multiset-based approaches to provide a more accurate and discriminative quantification of the stimulus recognition than the interiority and cross-correlation based methods. Significant differences in the specificity of the response have been observed in several cases, especially varying intensities, widths, and noise. Given their markedly more strict and discriminative characteristics, the real-valued and Jaccard, and even more so the coincidence approach, therefore correspond to the best choice, among the considered possibilities, for implementing more strict pattern recognition with high levels of accuracy.

There is an important issue to be further discussed here, and it regards the interplay between discriminative and tolerant (or invariant) performance. One first important point concerns the fact that these seem to be opposite properties, in the sense that a neuron that is too tolerant will provide no specific response, and vice versa. Another critical issue concerns the fact that, taken independently, neither of these two properties are necessarily good or bad. As in an engineering problem, the best solution will be that which best suits the specific requirements.

However, in the context of effective recognition of several types of patterns in typical applications, in presence of all the considered perturbations, perhaps the most proper solution is a balanced combination of discriminative and tolerant abilities. Actually, there is a formal solution to this duality between specificity and generality that is not so often realized. It concerns the fact that it is indeed possible to achieve both characteristics in a synergistic manner, not as a kind of trade-off or balance. This solution consists of having sets of neurons, each of which highly discriminative and specific, whose combined operation provides for the requested levels of tolerance and generalizations.

Thus, while each instance of the presented pattern will be accurate and specifically identified by successive individual cells, at the overall group level substantial tolerance will be achieved for several instances and perturbations of the presented stimuli. Nevertheless, this ideal architecture can only be achieved at expense of substantial informational resources, be then biological or artificial. These flexible *and* highly discriminative ensembles, which constitute the ideal solution for many circumstances, are henceforth denominated *synergistic neuronal systems*.

The immediate consequence of the above considerations is that it becomes critical to have the means for implementing strict, discriminative pattern recognition at the smallest informational and energetic expenses. From this perspective, the multised-based similarity identification constitute a particularly interesting resource given their conceptual and informationally simple operation, allied to their substantially more strict and discriminative operation as verified in this work with respect to several perturbations and in [26] with respect to coexisting patterns.

Interestingly, it has been proposed recently that the multiset operations can be implemented in extremely efficient manner in analog electronics, using only a few operational amplifiers and analog switches [32], which makes the mutiset-based approaches, and in particular the coincidence index, components of choice for the development of real-time pattern recognition systems.

It remains an issue of great interest to contemplate how befitted for implementation in biological hardware the multiset operations ultimately are.

10 Strictness Effect

In this section we study the effect of having more strict coincidence comparison, controlled by the parameter D, on the similarity values obtained with respect to the considered input perturbations.

Figure 30 illustrates the coincidence values obtained for $D = 1, 3, 5, 7, 9, 11$ respectively to relative displacement between the reference and input gaussians. It can be readily verified that the obtained coincidence values decrease steadily with D, indicating that progressively more strict comparisons imply in reducing the obtained coincidence values.

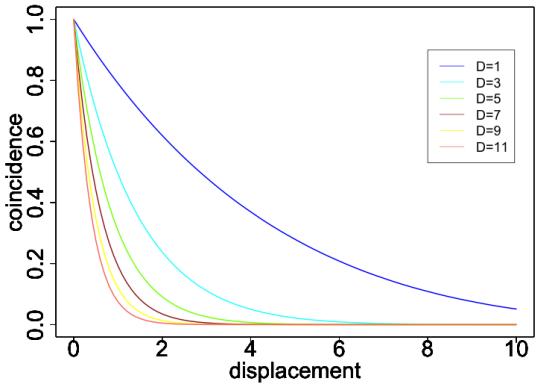

Figure 30: Similarity values obtained by the coincidence similarity for $D = 1, 3, 5, 7, 9, 11$ respectively to relative displacements of two identical gaussians.

The effect of increasing D on the coincidence values obtained with respect to modification of the intensity of

the input is shown in Figure 31. Again, the results indicate smaller indications of the presence of the reference pattern as the coincidence becomes more strict. Similar effect can be verified respectively to variation of the input width (Fig. 32), noise and interference.

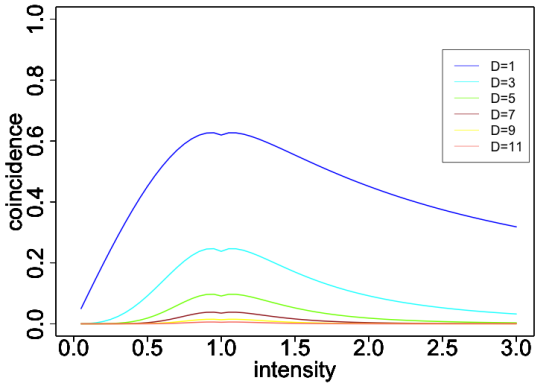

Figure 31: Quantification of the similarity between two circularly symmetric gaussians with the same dispersion, but one of them multiplied by a scaling factor from 0 to 3. The similarity values correspond to the coincidence index for $D = 1, 3, 5, 7, 9, 11$.

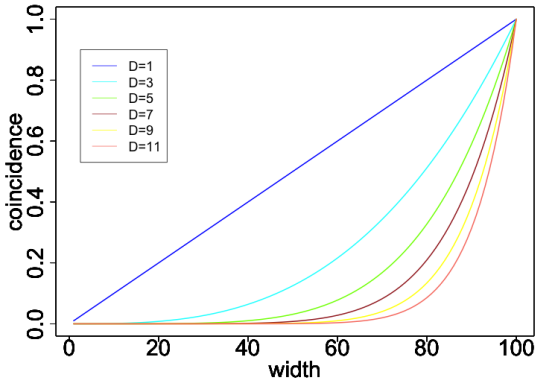

Figure 32: The coincidence similarity between the two patterns in terms of the variation of the width, corresponding to the standard deviation, of one of them.

task (e.g. [34, 35]). Basically, given an image containing several objects, as well as possibly a background, the task of *segmentation* consists in identifying the regions in the image that correspond to the objects of interest. Observe that image segmentation therefore corresponds to a *pattern recognition* problem in which each image pixel is to be classified as belonging or not to the objects of interest.

In the present section we illustrate the impressive potential of multiset neurons based on the real-valued Jaccard and coincidence similarity indices, for performing supervised image segmentation. For generality's sake, we will consider the RGB (color) image with size 300×319 pixels shown in Figure 33. The objects of interest will consist of the small leaves in the background of the image. Observe that these leaves have intense variation of hues, intensities, contrast and even focus, which contribute to making this problem a particular challenge. In particular, these leaves have tons of brown and red, in addition to green, which makes their separation from the other image objects especially difficult.

Figure 33: The image considered for illustrating the suggested multiset neuron based segmentation method. This RGB image has size 300×319 pixels, containing flowers against a varied background that includes small leaves with varying hues, intensity, contract and focus. The identification of the green leaves constitutes a particularly challenging problem in image processing and analysis.

11 Application Example: Image Segmentation

Among the several methods typically involved in image analysis, the segmentation of the objects of interest constitutes what is possibly the most difficult and challenging

The method proposed here, which is as simple as it is powerful, consists of taking a few samples of typical pixels belonging to the objects of interest, and then taking the R, G, and B values. A multiset neuron with hard limit output (see Fig. 22) will be assigned to recognize each of these N_s samples. The template vector of each of these neurons corresponds to the RGB values of the sampled pixel as well as of its w neighbors (e.g. within a

square of size $2w + 1$). Having thus trained the system, the image segmentation proper consists of obtaining the real-valued Jaccard or coincidence values by comparing the template with each of the image pixels for each of the multiset neurons, and the resulting similarity value is then thresholded by T (hard-limiting output function). In the present examples, no pre-processing is performed on the original image.

A logical or is then performed between the obtained outputs of the N_s neurons, and the original image pixel is understood to belong to the objects of interest whenever at least one of the neurons yields a true value. Several other types of features can be adopted, including statistics of the RGB values (e.g. average and statistical moments), as well as entropy and other indices, around each of the sample points.

Figure 34 illustrates the results obtained by taking just $N_s = 5$ pixels samples taken mostly at the lower right portion of the image, respectively to the real-valued Jaccard multiset neurons (a) with $T = 0.78$, and coincidence multiset neurons (b) with $T = 0.74$. For comparison's sake, a smaller threshold has been adopted in the latter case, since the coincidence is more strict than the Jaccard similarity. In both cases, we adopted $w = 1$, implying a total of $3(2w + 1)^2 = 27$ features (or number of synaptic inputs) for each neuron. The processing, which involves just the parameters T and w, took less than half a minute in a standard personal computer.

Though similar, the results obtained for the Jaccard and coincidence similarity present some differences that are consequence of the more strict quantification of the similarity between the pixel properties which is characteristic of the coincidence approach. Both results can be considered to be particularly satisfactory, involving minimal computational resources.

The segmentation of the cores and petals of the flowers by using a coincidence neuronal multiset network with $T = 0.78$ and $w = 1$ is illustrated in Figures 35 (a) and (b), respectively. Again, just $N_s = 5$ pixels were sampled from the flowers that are most at the forefront. Remarkable results have been again been obtained.

Figure 36 shows the segmentation of the flower cores with the same network as in Figure 35, but incorporating an output sigmoid function (Eq. 34) with $a = 20$ and $T = 0.83$, accounting for a graded resulted instead of the binary decisions implemented by the hard limiting function adopted in the previous examples. Observe that the additional obtained details appear with reduced intensity, which is a consequence of the sigmoid acting only on the similarity values resulting from the real-value coincidence

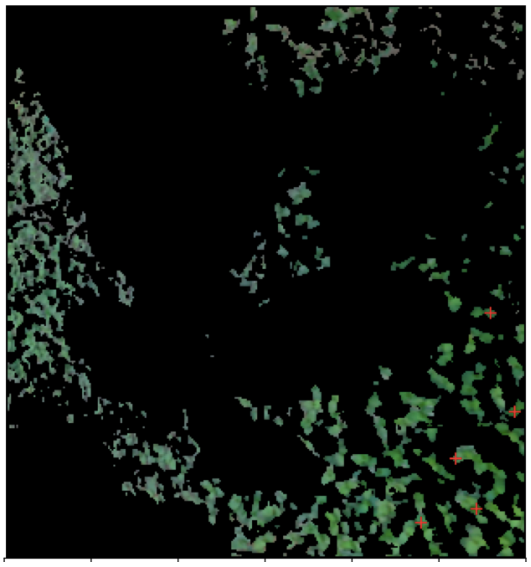

(a)

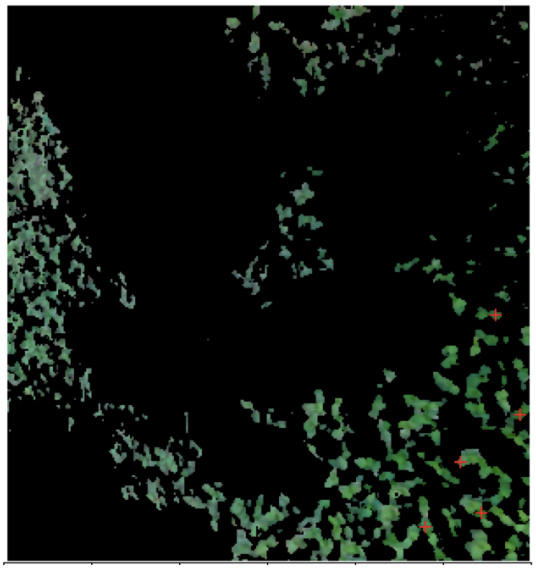

(b)

Figure 34: Segmentation of the small leaves in Fig. 33 obtained by using multiset neurons based on real-valued Jaccard (a) and coincidence (b) similarity with $w = 1$. Only 5 samples (pixels, marked by respective cross-hairs in the image) belonging to the objects of interest were used to train the system, which adopted $T = 0.78$ and $T = 0.74$ respectively to the Jaccard and coincidence approaches. The time required for training is just a few seconds, and the whole identification of the regions takes less than half a minute in a standard personal computer. The multiset neuronal network included only 5 neurons with sharp non-linear output.

The multiset neurons can also be applied to segment gray-level images as that shown in Figure 37(a). The segmentation results, using coincidence neurons with $w = 1$ and $T = 0.85$ are presented in Figure 37(b). The sample points being chosen at the brighter background, and the result was complemented in order to reveal the portions of the image that do not belong to the background.

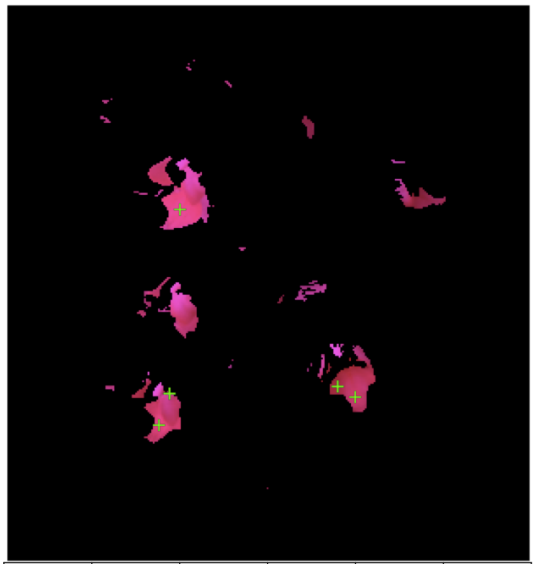

(a)

(b)

Figure 35: Segmentation of the cores (a) and petals (b) of the flowers in Fig. 33 obtained by a simple neuronal multiset network with $N_s = 5$ neurons based on the coincidence similarity, with $T = 0.8$ (cores), $T = 0.83$ (petals) and $w = 1$. The chosen samples are marked by the green cross-hairs.

Figure 36: Segmentation of the cores of the flowers in Fig. 33 obtained by a neuronal of generalized multiset network with $N_s = 5$ neurons with based on the coincidence similarity, with $T = 0.75$ and $w = 1$, incorporating a sigmoid output function with $a = 30$ and the same $T = 0.83$ as in Fig. 35. The pixels intensity is proportional to the estimated similarity with the trained pixels.

12 Concluding Remarks

The present work has developed a study of the application of the multiset-derived similarity operations, especially the real-valued Jaccard and coincidence indices, to artificial neurons. More specifically, these indices are considered for substituting the inner product performed between the image stimulus and respective matrix of synaptic weights.

After presenting an overview of the related multiset concepts and developments that led to the real-valued Jaccard and coincidence index, including new results regarding higher order respective versions, we proceeded to a systematic comparison of artificial neurons performing pattern recognition in presence of several types of perturbations. More specifically, the pattern to be recognized is stored in the synaptic weights, while the similarity comparison is performed by using the several considered indices.

The results largely confirm the enhanced potential of the coincidence index, followed by the real-valued Jaccard index, for performing strict similarity quantification. This makes these types of artificial neurons primary choices for implementations and applications involving strict patter recognition. The duality between specificity and generality in this type of task has also been discussed, and it has been argued that the ideal solution is to have large ensembles of highly specific and strict neurons, each of which adapted for taking into account specific geometric transformations so as to allow respective invariance.

Now, a particularly interesting issue arises regarding the fact that, given the substantial advantages of neurons based on the coincidence or real-valued Jaccard indices, why would they have not been adopted in biological neuronal networks aimed at effective pattern recognition? Why would the otherwise much less efficient inner product be instead implemented by the dendritic integration of the synaptic input?

There are at least two possible answers to this important question. First, we have that the biological hard-

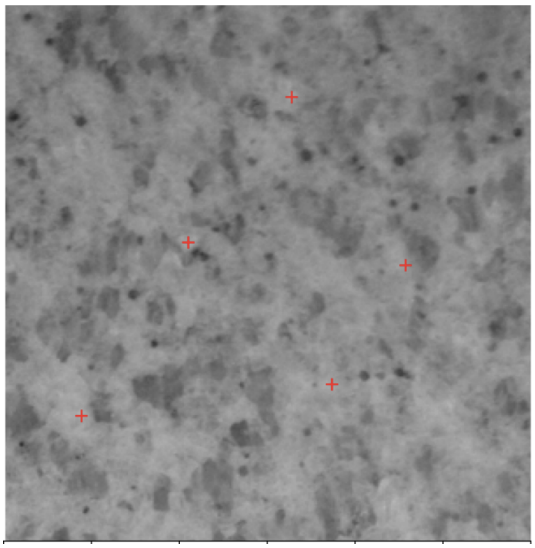

(a)

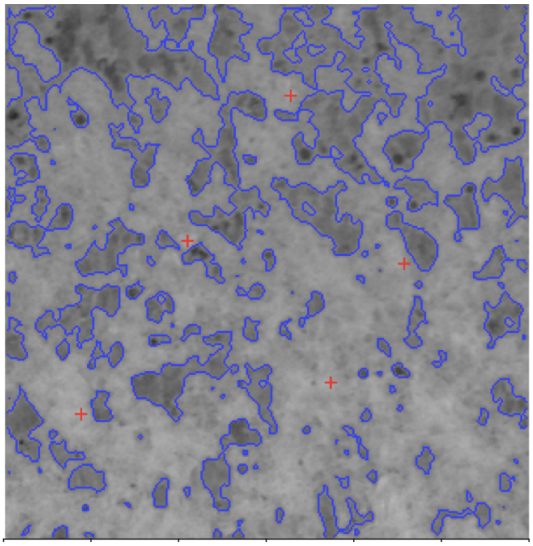

(b)

Figure 37: Segmentation of a gray level image (a) performed by a coincidence neuronal network with $N_s = 5$ samples (identified by the cross-hairs) and respective neurons with $w = 1$ and $T = 0.83$, with complementation of the logical or between the respective outputs being performed in order to reveal the objects that are not part of the background.

ware would be intrinsically unsuitable for implementing the multiset-related operations. Interestingly, recent developments have shown that these operations can be very effectively implemented in analog electronics [32], but this does not necessarily extend to biology, though much of the neuronal operation is a correlate of electric and even electronic counterparts. If it happens that biology is intrinsically unsuitable for performing multiset operations, these alternatives remain still valid for implementations in other types of hardware.

The second possible answer is that the biological neuronal cells actually implement multiset-related functions. Indeed, consider the profile of the operation $x \sqcap y$ shown in Figure 8, which is the basis for all effective indices developed and applied in the present work. This function, which resembles a sigmoid, could be applied not at the implantation cone, but at each of the synapses. Indeed, the observed saturation could correspond to the saturation of the synaptic activation and/or of the local polarization of the interior of the cell. The sum corresponding to the numerator of Equation 11 would then correspond to the combination of the diffusive charge effect at the implantation cone.

As for the denominator of that same equation, it is possible that other intracellular mechanisms are activated by the synaptic activity that effectively contribute to the inhibition of the action potential. These inhibitory effects could be similarity integrated at the implantation cone, accounting for the denominator in Equation 11. There are other possible mechanisms that could account for the implementation of multiset-like neuronal operations. For instance, the denominator of Equation 11 could correspond to inhibitory effects received from other cells associated to the same receptive field that would therefore counterbalance the net depolarization of the excitatory cell implementing the numerator integration.

Though these are currently hypothetical, further consideration and experimental developments can help verifying these possibilities.

The concepts, methods, and results reported in the present work have several potential implications in a wide range of areas — including neuroscience, pattern recognition and deep learning — therefore paving the way to a large number of further developments. Some examples include further studies of the possible relationships with biological cells, the consideration of other types of stimuli, as well as the evaluation of the here introduced higher order versions of the real-valued Jaccard and coincidence indices.

Acknowledgments.

Luciano da F. Costa thanks CNPq (grant no. 307085/2018-0) and FAPESP (grant 15/22308-2).

References

[1] S. Haykin. *Neural Networks And Learning Machines.* McGraw-Hill Education, 9th edition, 2013.

[2] Warren Mcculloch and Walter Pitts. A logical calcu-

lus of ideas immanent in nervous activity. *Bulletin of Mathematical Biophysics*, 5:127–147, 1943.

[3] D. H. Hubel and T. N. Wiesel. *Brain and Visual Perception: The Story of a 25-Year Collaboration*. Oxford University Press, Oxford, 2004.

[4] D. Hubel and T. Wiesel. Receptive fields, binocular interaction, and functional architecture in the cat's visual cortex. *Journal of Physiology*, 160:106–154, 1962.

[5] M. H. Turner, G. W. Schwartx, and F. Rieke. Receptive field center-surround interactions mediate context-dependent spatial contrast encoding in the retina. *eLife*, 7:eLife 2018;7:e38841, 2018.

[6] E. O. Brigham. *Fast Fourier Transform and its Applications*. Pearson, 1988.

[7] K. R. Rao, D. N. Kim, and J. J. Hwang. Integer fast fourier transform. In *Fast Fourier Transform - Algorithms and Applications. Signals and Communication Technology*, pages 111–126. Springer, Dorcrecht, 2010.

[8] A. V. Oppenheim and R. Schafer. *Discrete-Time Signal Processing*. Pearson, 2009.

[9] C. Phillips, J. Parr, and E. Riskin. *Signals, Systems and Transforms*. Pearson, 2013.

[10] S. Ramon y Cajal. *Recollections of My Life*. The MIT Press, Cambridge, Mass., 1996.

[11] R. Friedman. Measurements of neuronal morphological variation across the rat neocortex. *Neuroscience Letters*, 734, 2020.

[12] W. B. Grueber, C.-H. Yang, B. Ye, and Y.-N. Jan. The development of neuronal morphology in insects. *Current Biology*, 730–738, 2005.

[13] L. da F. Costa. On similarity. https://www.researchgate.net/publication/355792673_On_Similarity, 2021. [Online; accessed 21-Aug-2021].

[14] L. da F. Costa. Further generalizations of the Jaccard index. https://www.researchgate.net/publication/355381945_Further_Generalizations_of_the_Jaccard_Index, 2021. [Online; accessed 21-Aug-2021].

[15] L. da F. Costa. Coincidence complex networks. https://iopscience.iop.org/article/10.1088/2632-072X/ac54c3, 2022. J. Phys.: Compl, 3 015012.

[16] P. Jaccard. Distribution de la flore alpine dans le bassin des dranses et dans quelques régions voisines. *Bulletin de la Société vaudoise des Sciences Naturelles*, 37:241–272, 1901.

[17] Wikipedia. Jaccard index. https://en.wikipedia.org/wiki/Jaccard_index. [Online; accessed 10-Oct-2021].

[18] L. da F. Costa. Multisets. https://www.researchgate.net/publication/355437006_Multisets, 2021. [Online; accessed 21-Aug-2021].

[19] J. Hein. *Discrete Mathematics*. Jones & Bartlett Pub., 2003.

[20] D. E. Knuth. *The Art of Computing*. Addison Wesley, 1998.

[21] W. D. Blizard. Multiset theory. *Notre Dame Journal of Formal Logic*, 30:36—66, 1989.

[22] W. D. Blizard. The development of multiset theory. *Modern Logic*, 4:319–352, 1991.

[23] P. M. Mahalakshmi and P. Thangavelu. Properties of multisets. *International Journal of Innovative Technology and Exploring Engineering*, 8:1–4, 2019.

[24] D. Singh, M. Ibrahim, T. Yohana, and J. N. Singh. Complementation in multiset theory. *International Mathematical Forum*, 38:1877–1884, 2011.

[25] F. Gewers, G. R. Ferreira, H. F. Arruda, F. N. Silva, C. H. Comin, D. R. Amancio, and L. da F. Costa. Principal component analysis: A natural approach to data exploration. Researchgate, 2019. https://www.researchgate.net/publication/324454887_Principal_Component_Analysis_A_Natural_Approach_to_Data_Exploration. accessed 1-Oct-2020.

[26] L. da F. Costa. Comparing cross correlation-based similarities. https://www.researchgate.net/publication/355546016_Comparing_Cross_Correlation-Based_Similarities, 2021. [Online; accessed 21-Oct-2021].

[27] K. S. S. Kumar. *Electric Circuits and Networks*. Pearson Education India, 2009.

[28] B. Mirkin. *Mathematical Classification and Clustering*. Kluwer Academic Publisher, Dordrecth, 1996.

[29] C. E. Akbas, A. Bozkurt, M. T. Arslan, H. Aslanoglu, and A. E. Cetin. L1 norm based multiplication-free cosine similiarity measures for big data analysis. In *IEEE Computational Intelligence for Multimedia Understanding (IWCIM)*, France, Nov. 2014.

[30] C. E. Akbas, A. Bozkurt, A. E. Cetin, R. Cetin-Atalay, and A. Uner. Multiplication-free neural networks. In *Signal Processing and Communications Applications Conference (SIU)*, Malatya, Turkey, May. 2015.

[31] L. da F. Costa. Generalized multiset operations. https://www.researchgate.net/profile/Luciano-Da-F-Costa, 2021. [Online; accessed 10-Nov-2021].

[32] L. da F. Costa. Multiset signal processing and electronics. https://www.researchgate.net/publication/355954430_Multiset_Signal_Processing_and_Electronics, 2021. [Online; accessed 21-Nov-2021].

[33] M. K. Vijaymeena and K. Kavitha. A survey on similarity measures in text mining. *Machine Learning and Applications*, 3(1):19–28, 2016.

[34] L. da F. Costa. *Shape Classification and Analysis: Theory and Practice*. CRC Press, Boca Raton, 2nd edition, 2009.

[35] R. C. Gonzalez and R. E. Woods and. *Digital Image Processing*. Pearson, New York, 2018.